THESIS FOR THE DEGREE OF DOCTOR OF PHILOSOPHY IN NATURAL SCIENCE,
SPECIALISING IN CHEMISTRY

Alkali Release and Effects on Biomass Thermal Conversion Processes

Yaxin Ge

UNIVERSITY OF GOTHENBURG

Department of Chemistry and Molecular Biology
University of Gothenburg
Gothenburg, Sweden

Alkali Release and Effects on Biomass Thermal Conversion Processes

Atmospheric Science,
Department of Chemistry and Molecular Biology,
University of Gothenburg,
SE-412 96 Gothenburg,
Sweden

ISBN: 978-91-8009-927-1 (PRINT)
ISBN: 978-91-8009-928-8 (PDF)

Printed by Stema Specialtryck AB
Borås, Sweden 2022

Abstract

High alkali content is an important feature of biomass, and it has a series of implications for thermal conversion processes. This thesis focuses on the release of alkali during various biomass thermal conversion processes, including biomass pyrolysis, char gasification, co-conversion of different types of biomass, and thermal conversion of biomass mixed with fresh and used bed materials. Alkali release is also studied in combination with fuel conversion, to elucidate the underlying relationships. In addition, particle release during steam gasification of char is investigated.

The studies were carried out on different reactor scales, ranging from the micro scale to pilot scale. A reliable methodology for simultaneous monitoring of alkali release and sample mass was developed based on the application of a thermogravimetric analyzer in combination with a surface ionization detector (TGA-SID). Using TGA-SID, a significant level of alkali release was observed when wood char conversion approaches completion during CO_2 gasification, while the level of alkali release from straw char decreased continuously throughout the process. Alkali migration from straw to wood was observed at temperatures above 600°C during co-pyrolysis, based on online alkali measurements. Positive and negative synergistic effects were observed during the co-gasification at low and high conversions of char, respectively. This is attributed to alkali and silicon migration from the straw to the wood. Fresh bed materials affect wood and straw char gasification reactivities and rates of alkali release, and different bed materials may play different roles. For example, an alkali-containing bed material can enhance char gasification in the initial stage, a Si-containing bed material inhibits char gasification and alkali release at high conversions of char, an Al-containing bed material can inhibit char conversion when the char has a high silicon content, and Mg- and Ca-containing bed materials ensure that alkali persists in releasable form, thus favoring substantial alkali release from the char. Used silicon bed material has a coating layer that is abundant in Ca, Si, K, and Mg. These elements can migrate to the char surface during thermal conversion processes and affect char gasification.

In addition, a comprehensive system based on diluters, particle sizers, and SID has been successfully used for particle and alkali measurements in laboratory- and pilot-scale reactors. The laboratory-scale steam gasification system shows that the released levels of alkali and particles significantly increase when char conversion approaches completion. Using steam as the gasifying agent instead of CO_2 results in a higher level of alkali release during most of the gasification stage. Aerosol particles are also released during steam gasification, at rates that vary by more than one order of magnitude depending on the char composition.

The present study improves our understanding of alkali release, migration, and reaction during biomass thermal conversion processes. The acquired fundamental knowledge can be used for reactor design, co-gasification optimization, and selection of bed materials.

Keywords: Alkali, biomass, co-conversion, bed material, thermal conversion, online measurements.

Abstract (in Swedish)

En hög alkalihalt är en viktig egenskap hos biomassa, och den har en rad konsekvenser för termiska omvandlingsprocesser. Detta arbete fokuserar på alkaliutsläpp under flera termiska omvandlingsprocesser för biomassa, inklusive pyrolys, träkolförgasning, omvandling av blandningar av olika typer av biomassa och termisk omvandling av biomassa blandad med färska och använda bäddmaterial. Alkaliemission studeras också i kombination med bränsleomvandling för att ta reda på underliggande samband. Dessutom undersöks partikelutsläpp vid ångförgasning av träkol.

Studierna utfördes i olika reaktorer från mikro- till pilotskala. En metodik för att samtidigt detektera alkalifrisättning och provmassa har utvecklats baserat på en kombination av en termogravimetrisk analysator och en ytjoniseringsdetektor (TGA-SID). Med hjälp av TGA-SID observerades en anmärkningsvärd alkaliemission när kolomvandlingen närmar sig fullbordan under CO_2-förgasning av träkol, medan alkaliutsläpp från halmkol kontinuerligt minskade under hela processen. Alkalimigration från halm till trä observerades över 600 °C under sampyrolys med hjälp av online alkalimätningar. Positiva och negativa synergistiska effekter observerades under samförgasningen vid låg respektive hög omvandling av kol, vilket beror på alkali- och kiselmigrering från halm till trä. Färska bäddmaterial påverkar trä- och halmkolsförgasning i reaktivitet och alkalifrisättning, och olika bäddmaterial kan spela olika roller. Till exempel kan alkalihaltigt bäddmaterial förbättra kolförgasning i det inledande skedet, Si-innehållande bäddmaterial hämmar kolförgasning och alkalifrisättning vid hög omvandling av kol, Al-innehållande bäddmaterial kan hämma omvandling när kolet har ett högt kiselinnehåll, och Mg- och Ca-innehållande bäddmaterial kan göra att mer alkali överlever i aktiva former, och bidrar därmed till en hög alkalifrisättning. Använt kiselbäddmaterial har en ytbeläggning som innehåller Ca, Si, K och Mg, vilken påverkar kolförgasningen. Dessa ämnen kan migrera till kolytan och påverka termiska omvandlingsprocesser.

Dessutom har ett system baserat på spädare, aerosolpartikelmätare och SID framgångsrikt använts för partikel- och alkalimätningar i reaktorer i laboratorie- och pilotskala. Ångförgasning i laboratorieskala visar att träkol frigör anmärkningsvärda mängder alkali när kolomvandlingen närmar sig fullbordan under förgasningen. Användning av ånga som förgasningsmedel resulterar i en högre alkalifrisättning under större delen av förgasningssteget än vid användning av CO_2. Aerosolpartiklar frigörs också under förgasningen och halten av partiklar varierar med mer än en faktor tio beroende på kolets sammansättning.

Denna studie bidrar till en bättre förståelse för alkalifrisättning, migration och reaktioner under termiska omvandling av biomassa och ger grundläggande data som kan användas för reaktordesign, optimering av samförgasning och val av bäddmaterial.

List of publications

This thesis is based on the following studies, which are referred to in the text by their Roman numerals:

Paper I: Real-time monitoring of alkali release during CO_2 gasification of different types of biochar
Yaxin Ge, Saiman Ding, Xiangrui Kong, Efthymios Kantarelis, Klas Engvall, Jan B. C. Pettersson
Fuel 327 (2022) 125102.

Paper II: Online monitoring of alkali release during co-pyrolysis/gasification of forest and agricultural waste: Element migration and synergistic effects
Yaxin Ge, Saiman Ding, Xiangrui Kong, Efthymios Kantarelis, Klas Engvall, Jan B. C. Pettersson
Manuscript submitted to Biomass and Bioenergy.

Paper III: Impacts of fresh bed materials on alkali release and fuel conversion rate during wood pyrolysis and char gasification
Yaxin Ge, Saiman Ding, Wenan Zhang, Xiangrui Kong, Efthymios Kantarelis, Klas Engvall, Jan B. C. Pettersson
Manuscript submitted to Renewable Energy.

Paper IV: Effect of fresh bed materials on alkali release and thermogravimetric behavior during straw gasification
Yaxin Ge, Saiman Ding, Wennan Zhang, Xiangrui Kong, Klas Engvall, Jan B. C. Pettersson
Manuscript submitted to Fuel.

Paper V: Effects of used bed materials on char gasification: Investigating the role of element migration using online alkali measurements
Yaxin Ge, Saiman Ding, Xiangrui Kong, Efthymios Kantarelis, Klas Engvall, Marcus Öhman, Jan B. C. Pettersson
Fuel Processing Technology 238 (2022) 107491.

Paper VI: Alkali release behavior during steam gasification of char in a fixed bed reactor and its effect on reactivity
Saiman Ding, **Yaxin Ge** (co-first), Efthymios Kantarelis, Xiangrui Kong, Jan B. C. Pettersson, Klas Engvall
Manuscript in preparation.

Paper VII: A novel method for on-line characterization of alkali release and thermal stability of materials used in thermochemical conversion processes
Viktor Andersson, **Yaxin Ge**, Xiangrui Kong, Jan B. C. Pettersson
Energies 15 (2022) 4365.

Statement of contribution

Paper I: Yaxin Ge shares the first authorship with Saiman Ding, and Jan Pettersson is the corresponding author. Yaxin Ge conducted experiments, analyzed the data, and wrote the original manuscript. Saiman Ding helped with experiments and data analysis.

Paper II: Yaxin Ge shares the first authorship with Saiman Ding, and Jan Pettersson is the corresponding author. Yaxin Ge conducted experiments, analyzed the data, and wrote the original manuscript. Saiman Ding helped with experiments and data analysis.

Paper III: Yaxin Ge is the main author together with Jan Pettersson. Yaxin Ge conducted experiments, analyzed the data, and wrote the original manuscript.

Paper IV: Yaxin Ge is the main author together with Jan Pettersson. Yaxin Ge conducted experiments, analyzed the data, and wrote the original manuscript.

Paper V: Yaxin Ge is the main author together with Jan Pettersson. Yaxin Ge conducted experiments, analyzed the data, and wrote the original manuscript.

Paper VI: Yaxin Ge shares the first authorship with Saiman Ding, and Klas Engvall is the corresponding author. Yaxin Ge and Saiman Ding conducted experiments, analyzed the data, and wrote the original manuscript.

Paper VII: Yaxin Ge, as the second author, contributed some of the data to the paper. Viktor Andersson and Jan Pettersson are the main authors.

Other publications (not included in this thesis)

Paper A: Alkali release and gasification kinetics during gasification of biochar with different alkali contents
Yaxin Ge, Saiman Ding, Xiangrui Kong, Efthymios Kantarelis, Klas Engvall, Jan B. C. Pettersson
Manuscript in preparation.

Paper B: Alkali release during biomass thermal conversion under inert, reducing and oxidizing conditions
Yaxin Ge, Xiangrui Kong, Efthymios Kantarelis, Klas Engvall, Jan B. C. Pettersson
Manuscript in preparation.

Paper C:
Alkali interactions with a nickel-based catalyst for tar reforming in biomass gasification
Yaxin Ge, Xiangrui Kong, Viktor Andersson, Efthymios Kantarelis, Klas Engvall, Jan B. C. Pettersson
Manuscript in preparation.

Table of Contents

Part I
Summary

Chapter 1

Introduction

Environmental problems and energy shortages are major challenges facing society. Biomass, which is considered to be a renewable and more environmentally friendly resource compared to fossil fuels, is attracting more and more attention. Biomass currently supplies 14% of the world's energy and is the third largest energy resource in use [1–3]. The efficient use of biomass through thermal conversion technologies to produce heat, fuels, and chemicals is regarded as an important approach.

Compared to fossil fuels, biomass contains high concentrations of the alkali metals potassium (K) and sodium (Na) [4], which have multiple impacts on thermal conversion processes. For example, alkali metal-containing compounds are vaporized from biomass and subsequently participate in the thermal conversion process with catalytic effects. The vaporized alkali often re-condenses on the fly ash or heat exchanger surfaces to debilitate mass transfer [5]. Emitted alkali can also cause equipment corrosion, as well as the agglomeration and sintering of bed materials due to the low melting points of some alkali-containing compounds [4,6]. Moreover, certain high-cost downstream components, such as catalysts, fuel cells and turbines, may be sensitive to alkali [6–8]. Therefore, it is necessary to study alkali release and migration during biomass thermal conversion processes.

Co-conversion, e.g., co-pyrolysis and co-gasification, is a technology that is designed for efficiently converting fuels into chemicals and syngas. It has many advantages compared to the thermal conversion of single fuels [9,10]. Currently, studies of fuel co-conversion are mainly focused on coal-biomass blends [11–16], while the study of biomass-only fuel blends receives far less attention. During co-pyrolysis of biomass and coal, inorganic elements released from the biomass can catalyze the decomposition of heavy volatiles in the coal, resulting in a positive synergistic effect [17,18]. Regarding co-gasification, most earlier studies have reported that biomass blended with coal can improve the gasification reactivity compared to the individual fuels, and this is mainly attributed to the catalytic effects of alkali and alkaline earth metal (AAEM) species present in the biomass [19–22].

One commonly employed methodology for biomass thermal conversion is to use a fluidized bed for fluidization and efficient heat transfer. Several bed materials, e.g., dolomite, olivine, feldspar, and ilmenite, have shown positive effects on tar cracking and syngas quality [23–26]. In the case of bed materials that are used in a reactor for up to several days, an ash layer may form on the bed material particles due to the deposition of AAEM compounds released from the fuel [27–36]. The formed ash layer may, in turn, affect the thermal conversion of biomass [34,37].

Alkali release and migration take place during both biomass conversion and co-conversion of fuels, and they are important phenomena for the interactions between bed materials and biomass. An efficient method to characterize these dynamic processes is to employ online alkali measurements. Even though there have been several studies of alkali release during biomass gasification and combustion, there remains much to be learned due to the limited application of analytic tools for alkali metal monitoring with sufficient time resolution and the lack of systematic comparisons of different thermal conversion processes. Although a few studies have used online measurement methods to investigate alkali release during fuel pyrolysis in various atmospheres [38–40], knowledge gaps exist in several aspects, e.g., details about the alkali release kinetics and the relationship between alkali release and fuel mass loss. In addition, there is a scarcity of comprehensive reports on real-time monitoring of alkali release during the gasification of char, co-conversion of fuels, and thermal conversion of fuel mixed with bed materials.

The primary aim of this work is to contribute to an improved understanding of alkali release and its relationship to fuel reactivity during char gasification, co-conversion of different fuels, and thermal conversion of fuel mixed with bed materials. These themes are closely linked to the alkali-related issues in the corresponding industrial processes, e.g., catalytic functions, concentration in syngas, and migration between different materials. To link the sample mass and alkali release during thermal conversion processes, a novel experimental setup that connects a surface ionization detector (SID) for online alkali measurements to a commercial thermogravimetric analyzer (TGA) is developed. Based on the TGA-SID setup, alkali release during the gasification of different chars, the co-pyrolysis/gasification of wood and straw, the effects of fresh bed materials on wood and straw gasification, and the effects of used bed materials on industrial char are studied. In addition, a measurement system that comprises diluters, a CO/CO_2 analyzer, a scan mobility particle sizer, an optical particle sizer, and an SID, is successfully used for particle and alkali measurements in laboratory- and pilot-scale reactors.

Chapter 2

Background

2.1 Biomass and biomass thermal conversion

Biomass, which is a renewable energy resource, includes wood residues, agricultural residues, energy crops, and some industrial wastes [41,42]. Today, biomass is receiving more and more attention due to its carbon-neutral property [13]. Wood-based biomass is projected to cover up to 18% of the global energy needs in 2050 [3]. The utilization of biomass ranges from domestic heating to industrial-scale production of heat and power [43].

For the conversion of biomass into useful energy, thermochemical, biological, and mechanical methods are used. Thermochemical conversion is attracting intense interest because of its high efficiency, product diversity, and low level of waste residue [42]. Several thermal conversion technologies are being developed to enhance their efficiency and versatility. Pyrolysis, combustion, gasification, and hydrothermal processes are the basic approaches used for the thermochemical conversion of biomass [42]. The hydrothermal process disintegrates biomass in hot, high-pressure water to produce solid fuels with a low water content [42]. Pyrolysis is a process that decomposes biomass into tar, syngas, and char in an inert atmosphere at temperatures >350°C [42,44]. Biomass combustion is a well-established commercial technology that is based on the burning of biomass directly in air to generate heat and electricity [42]. Biomass gasification is a technology that is undergoing research and development to convert biomass into combustible synthesis gas (syngas) with quite high efficiency [44]. Gasifying agents, including CO_2, steam, and O_2, are used in the gasification to produce syngases with different compositions and purities [45].

Biomass gasification and pyrolysis are technologies that are under development [46]. Further development of the technologies is driven by identified needs to scale up the size of the reactor, increase the energy efficiency and fuel flexibility, and reduce the environmental risk, all of which benefit from detailed studies of the mechanisms underlying the thermochemical processes [47].

2.2 Alkali in biomass

Plants are one of the main sources of biomass. During growth, the plant absorbs some nutrients, including inorganic substances from the soil and air, resulting in relatively high concentrations of potassium and sodium in the biomass, as compared to conventional fossil fuels [48]. The potassium and sodium in biomass mainly comprise ion adsorbates, chemical adsorbates, and water-soluble salts [42]. They show high mobilities at high temperatures, and are easily released during biomass thermal conversion processes [49].

Alkali metals exert a variety of impacts on conversion processes. On a positive note, AAEMs in biomass can catalyze the thermal conversion of biomass [50–57]. During biomass pyrolysis, alkali reduces the decomposition temperatures of hemicellulose and cellulose, promotes tar cracking, and increases the gas yield [42]. It is also a good catalyst for depolymerization and other reactions, resulting in the formation of additional low-molecular-mass organic compounds [42]. During biomass gasification, alkali may act as a catalyst to enhance biomass gasification reactivity [58]. In the case of CO_2 gasification, an active intermediate involving alkali interacting with carbon may form, and this increases gasification reactivity, as shown in Figure 2.1 [49]. To clarify the catalytic effect of potassium during gasification, Dupont et al. investigated fuels with a high K-content and discovered that they had high gasification reactivities [59,60]. Suzuki et al. added K to chars, resulting in a remarkable increase in conversion rate at a char conversion above 80% [61]. In addition, a study of gasification rates at various K/C ratios has shown that the instantaneous conversion rate is proportional to the K/C ratio when the char conversion increases from 0% to 80% [62].

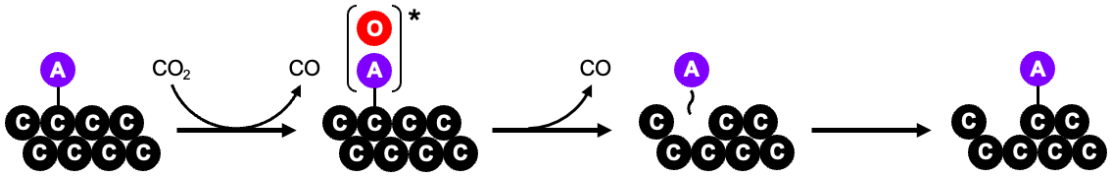

Figure 2.1 Schematic of the C-alkali interaction during CO_2 gasification, where "A" indicates an alkali atom [49].

Alkali released during the thermal conversion of biomass may cause a series of problems. For example, the evaporated alkali can subsequently be deposited on super-heater tubes, resulting in deterioration of heat transfer and corrosion of the equipment [6]. Ash with a high alkali content may have a low-melting point, causing sintering and agglomeration of the fluidized bed material [63]. Moreover, certain downstream components, e.g., catalysts, fuel cells and turbines, may be particularly sensitive to alkali [6,7].

Due to the positive and negative effects of alkali, many studies have focused on alkali release during the thermal conversion of biomass. During pyrolysis, alkali is released from the biomass in organic forms at temperatures <500°C and in inorganic forms at temperatures >500°C [39,40,42]. There are numerous studies of alkali release during pyrolysis, while less attention has been paid to alkali release during gasification. Hirohata et al. observed an increase in the release of AAEMs with increasing temperature during steam gasification of milled wood chips in a drop-tube reactor [64]. Some studies have shown an increase in alkali release with increasing degree of char conversion, especially at high degrees of char conversion [65,66]. Yang et al. have reported that 12–34 wt% of the alkali metals in the fuel are released during gasification of rice and corn straw, while most of the alkali in the remaining ash is in

the forms of carbonates, sulfates, and aluminosilicates [67]. There are also a few studies of online alkali release during biomass gasification. Fatehi et al. have identified two stages of alkali release associated with devolatilization and char reaction using laser-induced breakdown spectroscopy (LIBS) [68], while Zhang et al. have studied sodium [69] and potassium [70] release from sawdust particles during CO_2 gasification in a fluidized bed using inductively coupled plasma-optical emission spectroscopy (ICP-OES). However, there remain gaps in the knowledge related to alkali release during biomass gasification. For example, a comparison of alkali release from different biomasses and a correlation between fuel mass loss and alkali release are needed.

2.3 Co-conversion of fuels

Co-conversion of fuels is a potentially important approach to solving the problems associated with the conversion of individual fuels, e.g., low reactivity, ash melting, and alkali-induced corrosion [9,10]. Currently, extensive research is focused on the co-conversion of coal and biomass, including co-combustion [11–14], co-pyrolysis [15,18,71–77], and co-gasification [15,16], while the co-conversion of different types of biomasses receives less attention. In this thesis, we focus on studies of co-pyrolysis and co-gasification, as they have not been as-extensively applied in industries as co-combustion.

The presence or absence of synergistic effects in the co-pyrolysis of coal-biomass blends may depend on the fuel properties. Park et al. have reported that co-pyrolysis of sawdust and coal increases the gas yield and confers on the gas a high calorific value [71]. Krerkkaiwan et al. have observed that co-pyrolysis of straw and coal can produce chars with a higher surface area than the theoretical value calculated based on the two pure chars [74]. In contrast, studies carried out by Lu et al. and Ellis et al. have shown that the effects of co-pyrolysis on fuel mass loss and char structure are marginal [75,78]. Some studies have even found negative effects from the co-pyrolysis of biomass and coal, e.g., more large aromatic rings formed in the char [72,73] and a lower level of mass loss at temperatures <400°C [18].

Due to the catalytic effects of AAEMs in biomass, co-gasification of biomass and coal normally shows a higher reactivity than the calculated value based on the independent behaviors of these fuels [19–22]. Fernandes et al. have suggested that K can migrate from biomass particles to the surface of adjacent coal particles during pyrolysis and gasification, imposing catalytic effects on coal gasification [79]. However, the co-gasification of coal and biomass does not always show positive synergistic effects. Wei et al. and Zhang et al. did not observe any synergistic effect during the co-gasification of coal and biomass [21,22]. Some co-gasification studies using high-ash coals have even shown a reduction in gasification reactivity, owing to the fact that the ash of the coal deactivates the alkali in the biomass [80–82]. In addition, the effect of temperature on the synergistic effects of co-gasification appears

to be complicated, and different conditions, including low [83–85], moderate [86], and high temperatures [87], have been reported to promote synergistic effects.

At present, there are few published studies on the co-conversion of biomass-only fuel blends. Most of these studies have focused on the combustion of wood-straw blends, the properties of their ashes, and bed agglomeration [88–92]. In addition, a few studies have investigated the effects of biomass blends on the fuel conversion efficiency. Barmina et al. concluded that co-gasification and co-combustion of wheat straw and wood pellets could improve the conversion efficiencies [93]. Zhao et al. found that adding wheat straw to municipal solid waste during pyrolysis could result in an increase in the levels of CO and CO_2, but a decrease in the level of H_2 [94]. In a related work, Valin et al. compared the tar contents and gas compositions obtained during the gasification of several pure and blended feedstocks in a fluidized bed [95].

2.4 Effects of bed materials on biomass gasification

Fluidized beds are widely used for biomass thermal conversion. Therefore, bed materials are inevitably involved in biomass thermal conversion processes to provide efficient heat transfer and mixing [46]. Some bed materials also exert catalytic effects on the thermal conversion. This catalytic activity depends on the interactions between the biomass and bed material [96], and the interplay between these two elements needs to be carefully considered in the optimization of a conversion process.

Regarding the effects of the bed material on tar reforming and syngas quality, dolomite can not only catalytically crack tar, but it can also decrease the risk of bed agglomeration [23,26,97], while olivine shows a high catalytic activity for tar cracking [24], and ilmenite can induce tar cracking due to its high iron content [32,98].

Some recent studies have also shown that the outer ash layer on the used bed materials has catalytic effects on tar cracking and reforming [27–33]. The used bed material may have an outer ash layer after spending some time in a fluidized bed. Catalytic elements contained in the biomass ash [99], i.e., AAEM, are transported from the fuel particles to the bed material particles, leading to the formation of the ash layer by condensation, collision, and attachment [27–33]. He et al. [30,36] have shown that the thickness of the ash layer increases with an increasing number of operational days for bed materials collected from industrial bubbling fluidized bed (BFB) and circulating fluidized bed (CFB) boilers. Other studies have focused on the bed materials collected from gasifiers, e.g., olivine [34,35] and feldspar [100,101], and have found that a calcium-rich layer is formed after operation for approximately 1 day. The ash-coated bed materials may, in turn, release AAEMs to catalyze tar reforming during gasification. Ash-coated olivine that has experienced several days in a dual fluidized bed (DFB) can effectively reduce the tar content in a syngas and has a catalytic effect on the water-gas shift reaction [102–104]. A related study has shown that alumina also captures alkali metals released during biomass devolatilization and catalyzes tar cracking during biomass pyrolysis [105].

A few studies have begun to investigate the effect of the bed material on char gasification. A study conducted by Puig-Gamero et al. has shown that fresh dolomite can increase biomass char reactivity during steam gasification [106]. Keller et al. have demonstrated the catalytic effect of a potassium-soaked bed material on biomass char gasification, and noted the possibility of potassium migration from the bed material to the char [107]. Vilches et al. [34] have demonstrated that ash-coated olivine promotes a twofold increase in the gasification rate compared to fresh olivine, indicating potassium migration from the used olivine to the char particles. Lundberg et al. have shown that using ash-coated olivine as the bed material causes the char to have a much higher gasification reactivity than if using silica sand, owing to alkali migration [37]. However, some bed materials, e.g., sand, olivine, and dolomite, can have negative effects on char gasification, mainly because Si can react chemically with and deactivate the alkali [54,108]. As illustrated by these earlier studies, the effects of bed materials on char conversion are complex and warrant further study.

2.5 Alkali measurements during biomass thermal conversion

Several techniques have been applied to characterize alkali release during biomass thermal conversion. Currently used alkali measurement methods can be divided into offline and online methods. Offline methods extract and collect samples for subsequent analysis. One commonly applied offline method is to measure the sample mass and alkali content of partially converted chars. However, this method may have a limited time resolution and may be affected by changes in properties during sampling.

Online measurements are based on either in situ measurements or continuous gas extraction. There are a few examples of online alkali measurement techniques, including laser-induced fluorescence [109], LIBS [68], ICP-OES [69,70], plasma-excited alkali resonance line spectroscopy, molecular beam mass spectrometry [6,110], and surface ionization [111]. The SID used in this study has been applied previously in TGA experiments [47], laboratory-scale biomass pyrolysis [39,40,112], pilot-scale chemical looping combustion [113–117], and pilot- and industrial-scale biomass gasification [6,118,119]. The SID and other methods that rely on gas extraction, e.g., ICP-OES, face the challenge of alkali condensation on available surfaces when the gas is quenched and cooled. Considering these difficulties, there is a clear need for a system to evaluate alkali losses to high-temperature walls and during transportation in pipes at room temperature.

Chapter 3

Experimental methods

Several feedstocks and experimental setups are used in the investigations of alkali and particle release during thermal conversion. This section briefly introduces the different types of biomass, bed materials, reactors, instruments, and methodologies used in this thesis.

3.1 Materials

3.1.1 Biomasses

Four types of biomass with different origins were selected for use in the studies, including pine, a mixture of wood and branches, furniture waste, and straw. Table 3.1 shows the results of the proximate, ultimate, and ICP-OES analyses (mineral matter) of the used biomass materials. All the biomasses were used to investigate alkali release during biomass/char CO_2 and steam gasification (**Paper I** and **Paper VI**). Pine and straw were used in a co-pyrolysis and co-gasification study (**Paper II**). Pine

Table 3.1 Proximate, ultimate, and ICP-OES analysis of the biomasses.

Sample	Pine	Wood and branches	Furniture waste	Straw
Ultimate analysis (wt%, dry basis)				
C	50.9	47.3	48.7	42.9
H	6.20	6.47	6.10	5.86
N	0.10	0.06	4.08	0.48
O	42.8	46.2	41.1	50.8
S	0.01	0.00	0.04	1.62
Cl	< 0.02	-	0.016	-
Proximate analysis (wt%, delivered basis)				
Moisture	7.2	6.4	5.6	0.2
Volatiles	83.6	79.3	76.2	74.4
Ash	0.3	0.3	0.5	6.2
Fixed Carbon	8.9	13.9	17.7	19.2
Mineral matter (wt%)				
K	0.034	0.143	0.053	0.779
Na	0.011	0.003	0.013	0.013
Ca	0.056	0.120	0.115	0.200
Si	0.004	0.002	0.010	0.616
P	0.004	0.007	0.001	0.026
Al	0.008	0.002	0.003	0.008
Ba	0.000	0.001	0.001	0.004
Fe	0.005	0.001	0.002	0.007
Mg	0.011	0.015	0.011	0.052
Mn	0.007	0.005	0.009	0.002
Zn	0.001	0.001	0.001	0.001
Others	<0.001	<0.001	<0.001	<0.001

was used in a fresh bed material study (**Paper III**), and straw was used in a second fresh bed material study (**Paper IV**).

3.1.2 Entrained flow gasifier chars

Table 3.2 shows the results of the proximate, ultimate, ICP-OES (mineral matter), and BET (Brunauer-Emmett-Teller; surface area) analyses of the chars used in the studies. The original char (OC) was collected from a demonstration-scale entrained flow gasifier that used pine wood as feedstock [120]. The LC2 and LC48 samples were produced by washing the OC in distilled water for 2 h and 48 h, respectively. KCl-added char (AC) was prepared by adding a specific amount of KCl to the OC. The four samples were used to examine the effects of the alkali contents of the chars on alkali release and char gasification (Section 4.1.3). In addition, OC was used in the used bed material study (**Paper V**) and steam gasification study (**Paper VI**). It should be noted that the OC (also termed as industrial char) used in all TGA experiments was heated for 3 h at 950°C in an N_2 atmosphere [120].

Table 3.2 Results from the proximate, ultimate, ICP-OES, and BET analyses of the used chars.

Sample	LC48	LC2	OC	AC*
Proximate analysis (wt.%, dry basis)				
Moisture	0	0	0	0
Volatile Matter	3.5	4.0	4.5	≈ 4.5
Ash	3.4	5.3	6.9	≈ 6.9
Fixed Carbon	93.1	90.7	88.6	≈ 88.6
Ultimate analysis (wt.%, dry basis)				
C	87.92	87.28	85.77	≈ 85.77
H	0.88	0.95	1.12	≈ 1.12
N	0.36	0.36	0.37	≈ 0.37
S	0.06	0.07	0.09	≈ 0.09
O	10.78	11.34	12.66	≈ 12.66
Mineral content (mg/kg, dry basis)				
Na	173	495	755	≈ 755
K	766	3060	5690	≈ 8307
Mg	2350	2600	2660	≈ 2660
Ca	9320	10200	11200	≈ 11200
Fe	599	616	720	≈ 720
Al	330	350	336	≈ 336
Mn	1530	1550	1540	≈ 1540
P	693	701	677	≈ 670
Si	846	1930	1450	≈ 1450
Specific surface area (m^2/g)	410 ± 2.56	410 ± 2.16	330 ± 1.87	-

* The values for KCl-added char (AC) are calculated based on the original char (OC) and the added amount of KCl.

3.1.3 Fresh bed materials

Table 3.3 shows the mineral contents of the fresh bed materials used in the thesis. Silica particles were produced from colloidal silica (SiO_2, LUDOX® AS-40 colloidal silica; Sigma-Aldrich). Colloidal silica, sea sand, and alumina are pure chemicals provided by Sigma-Aldrich, although they still contain some impurities, e.g., K and Ca. Olivine (Sibelco Nordic AS, Åheim, Norway), ilmenite (Titania A/S, Hauge, Norway), and dolomite (White marble S0, 2-1; Björka Mineral AB, Sweden) are natural ores with more impurities. They were calcinated before use in the experiments, so as to remove releasable matter (for details, see **Papers III** and **IV**).

Table 3.3 Mineral content analysis using ICP-OES for the fresh bed materials.

Bed material	Silica	Sea sand	Olivine	Ilmenite	Alumina	Dolomite
Mineral matter (wt %)						
Al	0.026	0.101	0.53	0.38	49.4	0.67
Si	46	47.6	19.6	1.12	<0.04	2.93
Ca	<0.1	<0.05	0.36	0.20	<0.2	26.9
K	0.001	0.054	-	0.06	0.002	-
Na	0.105	0.138	-	0.03	0.203	-
Ti	0.005	0.023	-	26.7	<0.001	-
Fe	0.007	0.002	5.6	25.9	0.001	0.63
Mg	0.001	0.003	28.2	1.974	<0.001	22.6
P	<0.007	<0.005	-	-	0.011	-
Others	<0.0003	<0.0003	-	-	<0.0003	-
Surface area （m^2/g）	125	< 0.2	< 0.2	< 0.2	< 0.2	5.0

3.1.4 Used bed materials

Six bed materials were used to investigate the effects of used bed materials on char gasification. The bed materials were collected from a 30-MW_{th} BFB and a 90-MW_{th} CFB boiler [36]. The three BFB bed material samples were collected after operating the boiler for 7, 13 and 23 days, respectively. The three CFB bed materials were collected after operating the boiler for 1, 5, and 13 days, respectively. The fresh bed materials consisted of 80% quartz and minor fractions of the feldspar microcline and albite. The average particle sizes of the CFB and BFB bed materials were 200–500 μm and 700 μm, respectively [31,36]. The fuel used in the two boilers was softwood. The six used bed materials were investigated in **Paper V**.

3.2 TGA-SID setup

The SID used for the online alkali measurements was connected to a commercial TGA for measuring sample mass at high temperatures, creating the TGA-SID setup used in the studies. Two different TGAs were involved, as the experiments were done in different laboratories. The TGAs, located at KTH and Chalmers, were connected to the same SID, generating the KTH setup and Chalmers setup, respectively. The KTH setup was used in most of the studies related to biomass

thermal conversion, including those reported in **Papers I–V**. The Chalmers setup was used for developing the methodology described in **Paper VII**.

3.2.1 KTH setup

An SID was connected to a TGA to construct the TGA-SID setup shown in Figure 3.1. The SID, which was developed at the University of Gothenburg, is based on the natural phenomenon that alkali metal atoms have a high probability to desorb in ionic form from a hot metal surface [121]. It is used for sensitive and highly selective online measurements of the total concentrations of alkali, i.e., K and Na. The SID has been thoroughly described in the literature [122,123]. SID calibration is carried out using KCl aerosols of known concentrations [124].

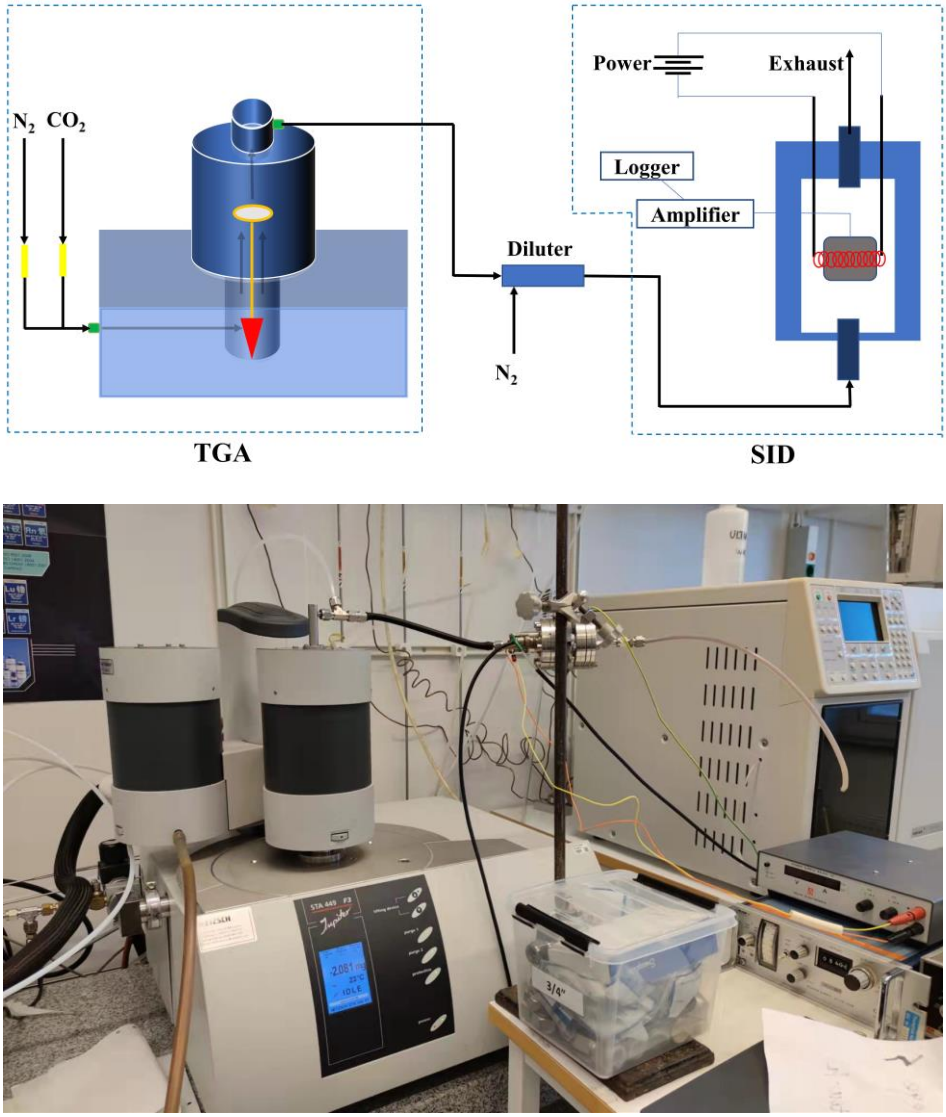

Figure 3.1 Schematic view and photograph of the TGA-SID system at KTH Royal Institute of Technology.

The KTH setup used the TGA instrument (model STA 449 F3; Netzsch GmbH, Selb, Germany). The flow into the TGA consisted of 80 ml/min N_2 as balance gas and 320

ml/min of the reaction gas. The reaction gas was either pure N_2 or a mixture of N_2 and CO_2, resulting in 0%, 15% or 30% CO_2 in the total gas flow. After the TGA outlet, a diluter was connected to increase the flow to the working flow of the SID, which is 700 ml/min. The sample was loaded into the TGA for each experiment and heated from room temperature to a high temperature (850°C, 900°C or 950°C) with a constant heating rate of 20°C/min in pure N_2. This was followed by gasification in CO_2 for 20–100 min depending on the sample, reaction temperature, and pre-treatment processes. For the co-gasification and bed material experiments, the mass of each material was precisely measured, and the material was thoroughly stirred to ensure uniform mixing.

3.2.2 Chalmers setup

The Chalmers setup used a TGA of model Q500 (TA Instruments Inc., New Castle, DE). A schematic of the setup is presented in Figure 3.2. The gas flow into the TGA device consisted of 10 ml/min N_2 as balance gas and 90 ml/min of environmental gases, i.e., inert, oxidizing and reducing gases. After the TGA outlet, a diluter was connected that diluted the exhaust flow by a factor of seven before the flow entered the SID at a flow rate of 700 ml/min. For each experiment, a 10-mg sample was loaded and heated from 25°C to 1000°C at a heating rate of 5, 10 or 15°C /min. Subsequently, isothermal experiments at 1000°C were typically performed for 1 h, to observe the rate of decline of alkali release as a function of time. The TGA flow of this setup was significantly lower than that of the KTH setup, resulting in longer residence times in the furnace and sampling lines and a higher likelihood of alkali condensation on the inner walls of the experimental setup. Based on the Chalmers setup, characterization and development of the TGA-SID methodology, including assessments of alkali loss in the tubes and reactor and calibration methods, were conducted (for details, see **Paper VII**).

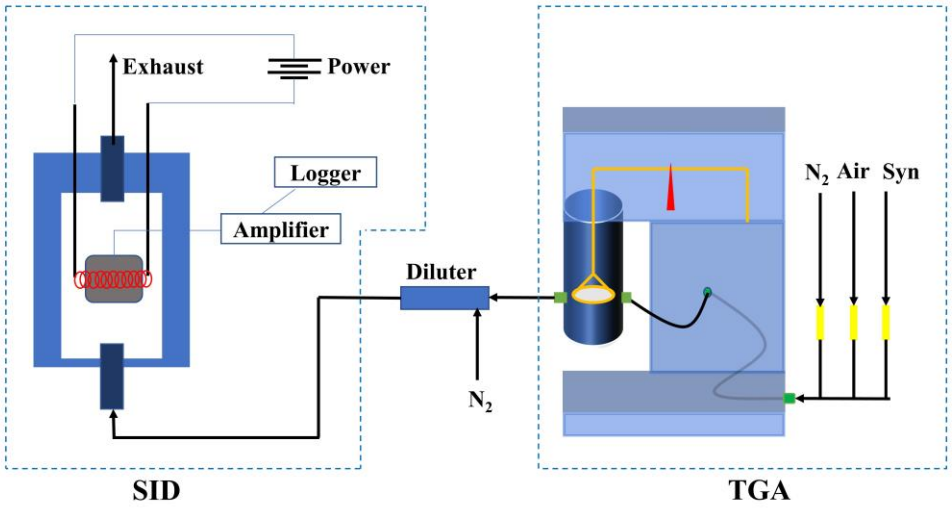

Figure 3.2 Schematic of the TGA-SID system at the Chalmers University of Technology.

3.3 Laboratory-scale fixed bed system

The release of alkali and aerosol particles during steam gasification of biomass and char samples were investigated using the system shown in Figure 3.3. The reactor consisted of a stainless tube with an inner diameter of 1.7 cm and a length of 40 cm. Samples were placed on a plate with 20-μm apertures, which was supported by another stainless tube with a diameter of 14 mm and a length of 30 cm to the upper part of the reactor. The distance from the sample to the exit portal of the reactor was kept short, to minimize interactions between the alkali metal compounds emitted from the sample and the hot reactor wall. At the outlet of the reactor, a diluter with a dilution ratio of 11 was connected to avoid particle and alkali concentrations that exceeded the measurement ranges of the instruments. After the outlet of the diluter, a manifold was connected to split the gas flow to a CO/CO_2 analyzer (model NGA 2000; Emerson Inc., St Louis, MO), an SID, a scanning mobility particle sizer (SMPS; model 3936; TSI Inc., Shoreview, MN), and an optical particle sizer (OPS; Dust Monitor model 1.108; GRIMM Aerosol Technik GmbH, Ainring, Germany). Steam was added by allowing the inlet gas to flow over a water bath that was maintained at 42°C, which resulted in a water vapor concentration of around 8%. For each test, 0.5 g of sample was placed in the reactor, followed by heating in pure N_2 to the desired temperature for gasification (800°–950°C). The reactor was then kept under isothermal conditions for a short time (10–20 min) to stabilize the system, before steam gasification was initiated by switching to N_2 gas that contained steam. The gasification process proceeded until the measured CO concentration was <10 ppm.

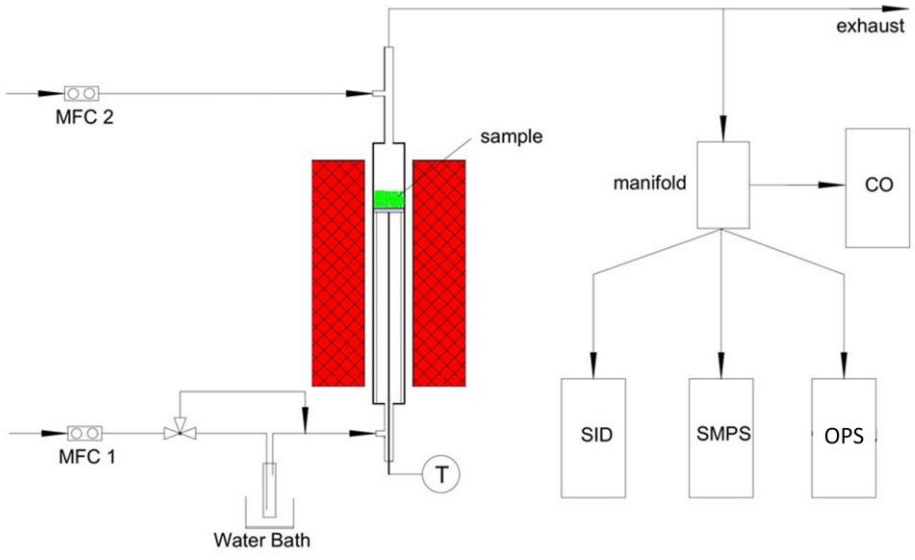

Figure 3.3 Schematic of the laboratory-scale fixed bed reactor setup used for the steam gasification experiments.

The SMPS was used to measure the size distribution of aerosol particles. The SMPS system consists of a differential mobility analyzer (DMA model 3080; TSI) operating

in recirculation mode and connected to a condensation particle counter (model 3010; TSI). The aerosol and sheath flow rates in the SMPS were 1.0 and 5.0 l/min, respectively, resulting in a measured particle diameter range of 10.7−487.0 nm.

The OPS is a portable instrument that enables continuous measurement of particle numbers and mass concentrations with a high time resolution. The particles pass through a light source and the scattered signal is transferred to a recipient diode [125].

3.4 KTH 75-kW pressurized gasifier

Figure 3.4 shows a schematic of the pilot-scale pressurized gasifier at KTH Royal Institute of Technology. This setup was used to study alkali, particle, and sulfur release during steam or O_2 gasification of biomass at high pressure conditions.

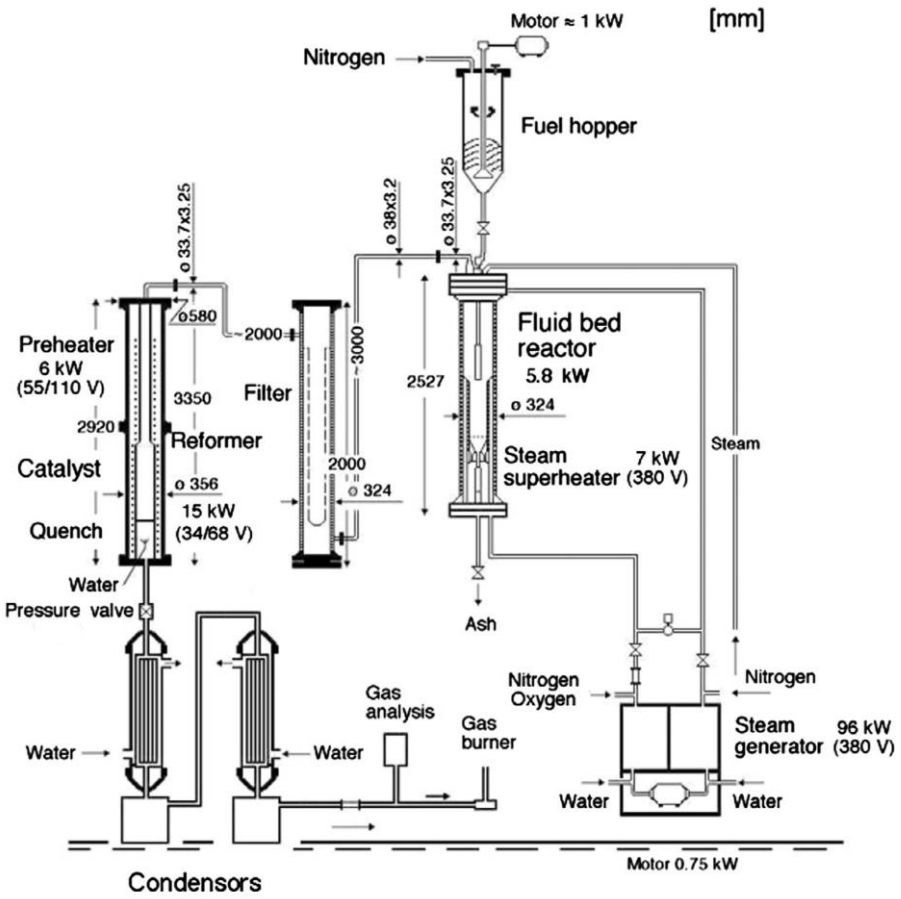

Figure 3.4 Schematic view of the pressurized gasifier at KTH Royal Institute of Technology [23].

The gasifier consists of a steam generation boiler, a pressurized fluidized bed reactor, a high-temperature filter, and a secondary reformer reactor. The designed maximum operating pressure and fuel feeding rate of the gasifier are 3.0 MPa and 15 kg/h, respectively [23]. On top of the fluidized bed reactor is a fuel hopper with a volume of 120 liters. The feed rate of fuel is controlled by the size of a slot opening and the stirring speed of the paddle in the hopper [23]. To ensure that the feeding process is smooth, N_2 is injected into the hopper to ensure a slight overpressure and to cool

down the feeding pipe [23]. During the experiments, the reactor temperature and bed pressure were monitored continuously [23]. The maximum operating temperature of the reactor is 950°C [23]. Oxygen, nitrogen and steam were fed directly into the reactor bottom, and additional steam was passed over the outer surface of the freeboard, so as to prevent overheating in the freeboard before entering the bottom of the reactor [23]. The filter and reformer have maximum operating temperatures of 500°C and 1100°C, respectively [23].

To analyze the syngas produced by the gasifier and the effect of the filter, the sampling system shown in Figure 3.5 was connected before or after the filter, using valves to switch the syngas lines. The gas flow in the inlet of the sampling chamber shown in Figure 3.5 was controlled to be 10 l/min by adjusting a needle valve in the inlet. A probe with an inner diameter of 4 mm was inserted into the sampling chamber and extracted 1 l/min syngas to the dilution system. The remainder of the sampled gas was vented to the exhaust and a gas chromatograph (GC), which was used to measure the gas composition. The extracted gas passed through three diluters, i.e., one diluter using a perforated tube for dilution and two ejector diluters (model D-1000; Dekati Ltd., Tampere, Finland) [118,122], to ensure a total dilution factor in the range of 100–300. A manifold was connected after the three diluters to distribute the gas into different instruments. The instruments, with the exception of those used for sulfur measurements, have been described in Section 3.3. The precise dilution ratio was calculated using the GC data (before the diluters) and the CO/CO_2 data (after the diluters).

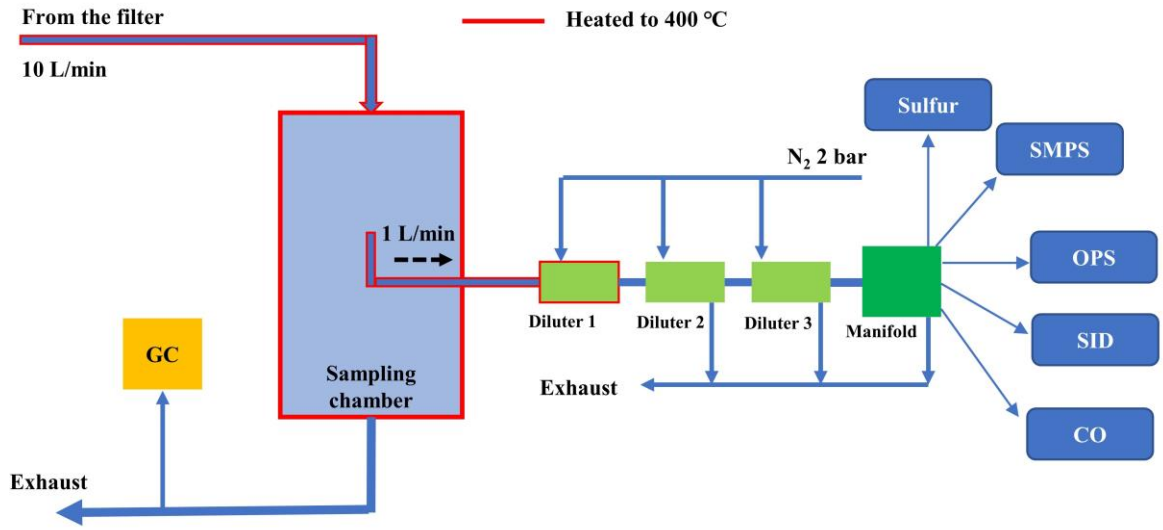

Figure 3.5 Schematic of the alkali, particle, and sulfur sampling systems.

3.5 SEM-EDS analyses

Scanning Electron Microscopy with Energy Dispersive Spectroscopy (SEM-EDS) was used to measure the relative contents of elements, e.g., K, Na, Al, Mg, Ca, Si, Ti, on the surfaces of the materials used in the studies. The samples for SEM-EDS

measurement were collected after gasification for a few minutes in 15% CO_2 at 900°C, i.e., the degree of char conversion around 0.3. The morphology assessed by SEM (Phenom ProX Quanta 200 FEG) was used to distinguish the wood char surface from the straw or bed material surface (**Papers II–V**). A few areas were randomly selected from different wood particles for the EDS analyses (Oxford Instruments) in the co-conversion study (**Paper II**) and the two fresh-bed material studies (**Papers III** and **IV**). In the used bed material study (**Paper V**), global scanning with amplification of 400× was used for the EDS (Oxford) analyses. The analyses were performed in low vacuum mode with carbon tape placed under the sample. A photograph of the employed instrument is shown in Figure 3.6.

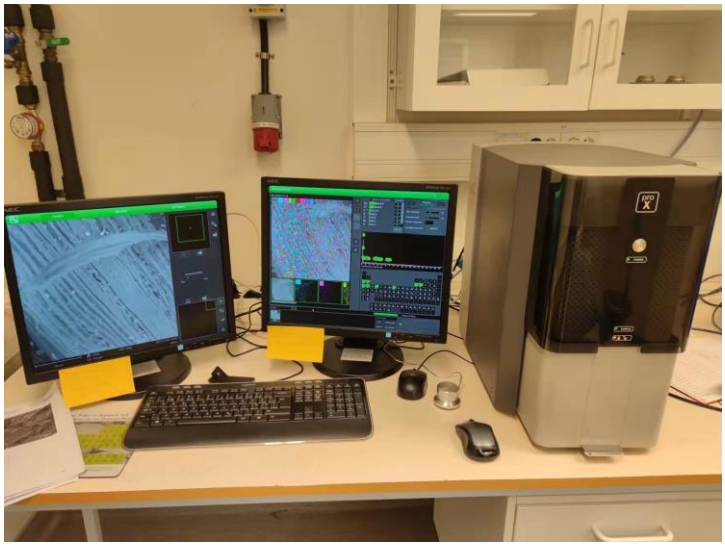

Figure 3.6 Photograph of SEM-EDS setup.

3.6 Data analysis

To analyze the char gasification stage, the following parameters were calculated and used in the studies.

The TGA results are used to calculate the conversion (X) of a biomass char during CO_2 gasification at a given time t using the following equation:

$$X = \frac{m_0 - m_t}{m_0 - m_f} \quad (1)$$

where m_0 is the initial mass of the sample when CO_2 is injected, m_t is the mass of the sample at a given time, and m_f is the final sample mass.

The reactivity of gasification is expressed as a conversion rate, r (s^{-1}) [126]:

$$r = \frac{dX}{dt} \quad (2)$$

The alkali release rate (A) is derived from the alkali concentration (C) measured by the SID and the total flow (F) of the SID, according to:

$$A = C \times F \quad (3)$$

In the co-conversion study (**Paper II**), the calculated sample mass (i.e., theoretical sample mass, m_{cal}) of the wood and straw mixture at a given time t was obtained based on results for pure wood and straw at a given time of reaction, using the following equation:

$$m_{\mathrm{cal}} = m_{\mathrm{w}} f_{\mathrm{w}} + m_{\mathrm{s}} f_{\mathrm{s}} \quad (4)$$

where m_w and m_s represent the wood and straw masses at time t, and f_w and f_s represent the initial fractions of wood and straw in the blend.

In a similar manner, the calculated alkali release rate (i.e., theoretical alkali release rate, A_{cal}) of the mixtures at time t was obtained using the following equation:

$$A_{\mathrm{cal}} = A_{\mathrm{w}} f_{\mathrm{w}} + A_{\mathrm{s}} f_{\mathrm{s}} \quad (5)$$

where A_w and A_s represent the instantaneous alkali release rate for wood and straw, respectively.

Synergistic effects at a certain conversion X during the isothermal co-gasification may be expressed by a synergy index (SI) [21,22,127]:

$$SI = \frac{t_{X,\mathrm{cal}}}{t_{X,\mathrm{exp}}} \quad (6)$$

where $t_{X,cal,}$ and $t_{X,exp}$ denote the calculated and experimental gasification times required to reach a conversion X, respectively. A positive synergistic effect during co-gasification results in an SI >1, and a higher SI indicates more-pronounced synergistic effects [21].

Chapter 4

Results and discussion

This chapter presents the main results from the studies of this thesis. Sections 4.1 to 4.4 present the results obtained from experiments carried out with the TGA-SID setup. The content starts with the conversion of pure biomass, followed by the results for the conversion of biomass mixed with another type of biomass or bed material. Section 4.5 describes the results obtained from the steam gasification experiments conducted in the laboratory-scale reactor. Section 4.6 reports the results obtained from the pressurized gasification experiments conducted in the KTH 75-kW gasifier. Some necessary discussions are included in the corresponding Results section. For details, see the indicated papers in each section.

4.1 Alkali release and mass loss during CO_2 gasification of biomass

This section presents the results for alkali release and char reactivity during CO_2 gasification of different chars, and includes studies of the effects of temperature, CO_2 concentration, and sample alkali content. A preceding pyrolysis stage is briefly described here because it is the char production process. The experiments were performed using the setup presented in Figure 3.1. See **Paper I** for details regarding Sections 4.1.1 and 4.1.2.

4.1.1 Alkali release during pyrolysis and gasification of biomass

Figure 4.1 shows the real-time data for sample mass and alkali release during pyrolysis and gasification of the four types of biomass listed in Table 3.1. The biomass pyrolysis stage shows a large mass loss, which is consistent with the high content of volatile matter and the low content of fixed carbon of the materials, as presented in Table 3.1. The dehydration of biomass results in a small peak in the mass loss rate in the temperature range of 60–120°C (Figure 4.1b), while no alkali release is observed in the same temperature interval (Figure 4.1, c and d). The temperature range of 200–400°C is the devolatilization stage [39,40]. Massive loss of mass and clear alkali release are observed for all the types of biomass in this stage. At temperatures >400°C, the alkali release rapidly decreases but remains detectable until 500°C, as shown in Figure 4.1, c and d. When the temperature increases from 500°C to 900°C, there is no obvious mass loss and no significant alkali release in the case of woody biomasses. The straw shows a different alkali release behavior above 600°C, i.e., the alkali release increases with increasing temperature and declines during the isothermal stage in N_2 at 900°C. This difference may be attributed to the high alkali content of the straw, as listed in Table 3.1.

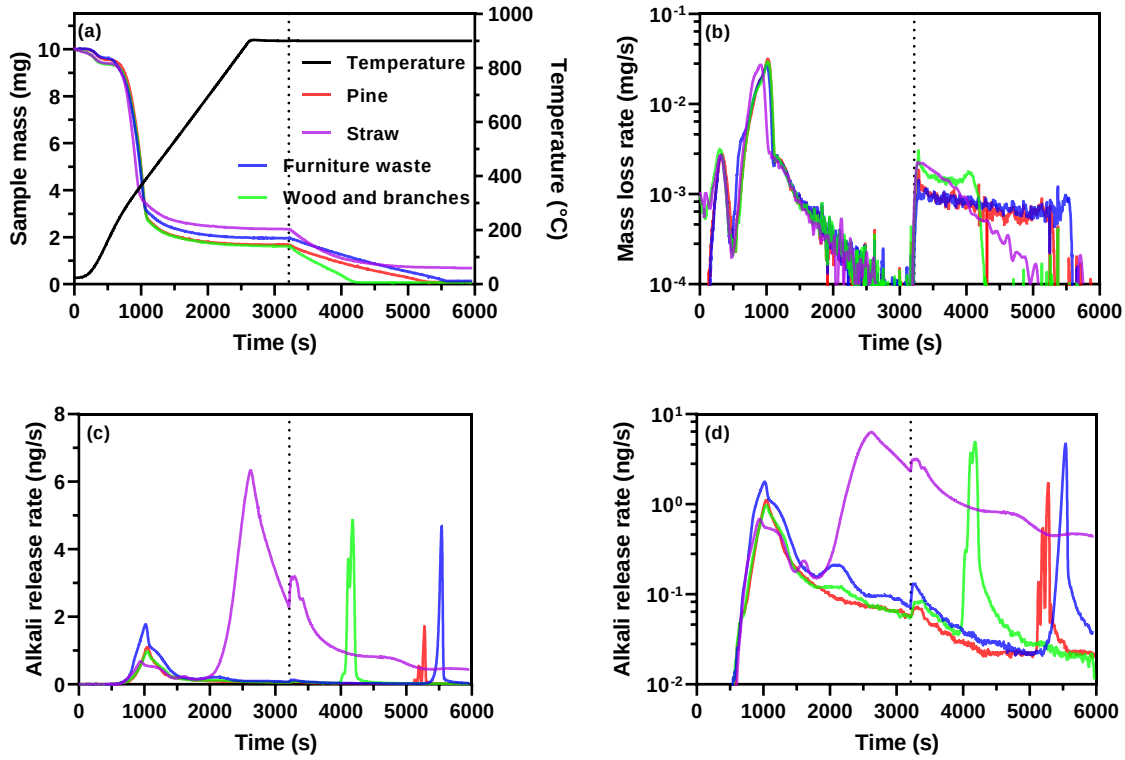

Figure 4.1 (a) Sample mass, (b) mass loss rate, and (c, d) alkali release rate during the pyrolysis of four biomass samples in pure N_2 and char gasification in 15% CO_2. The temperature profile is included in panel (a). Panel (d) displays the same data as in panel (c) using a logarithmic *y*-axis. Gasification was initiated by switching the gas composition from pure N_2 to 15% CO_2 in N_2 at the time indicated by the dotted line.

The char gasification stage is initiated by CO_2 injection, and the results are shown on the right side of the dotted line in each panel. Figure 4.1, a and b show that the mass loss rate increases immediately for all the samples when CO_2 is introduced. The three woody samples maintain a relatively high, albeit slowly decreasing, mass loss rate until gasification approaches completion. In the gasification completion stage, a minor increase in the rate of mass loss is observed. This increase has been reported in other studies [61,108,128], and is believed to be due to an increasing alkali concentration in the wood char during gasification [129]. The straw char shows a completely different mass loss behavior, whereby the mass loss rate continuously decreases throughout the gasification process. The amount of alkali released from the three woody chars is very low and shows a decaying trend during most of the gasification stage. However, a remarkable release of alkali occurs when the char gasification approaches completion. This is related to the gradual accumulation of alkali in the chars [61,66], which is eventually released from the samples during the final stage of gasification (for details, see the *Discussion* section of **Paper I**). Similar results were found in a gasification study of K-loaded lignite char using an offline alkali measurement method [130]. The pronounced alkali release is followed by a rapid decrease in the level of alkali emission. In contrast, straw shows a high level of

alkali release at the beginning of gasification and this level continuously decreases throughout the process.

4.1.2 Effects of temperature and CO_2 concentration

The comparison of mass loss and alkali release during pyrolysis of pine and isothermal gasification of pine char with different final temperatures (850 – 950 ˚C) is shown in Figure 4.2. The mass and alkali release curves almost overlap during pyrolysis, indicting a high reproducibility of the experiments. The char masses are almost the same when injecting CO_2 to initiate gasification. The time required to complete char gasification becomes shorter with increasing gasification temperature and a high temperature thus helps to accelerate the gasification process [131]. The alkali release rate slightly increases in most of the gasification stage and increases remarkably when the char conversion approaches completion.

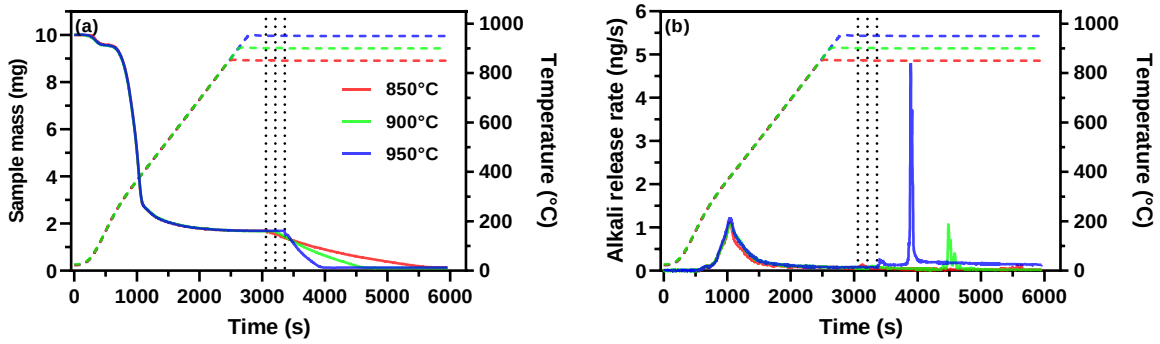

Figure 4.2 (a) Sample mass and (b) alkali release during pine heating in N_2 and isothermal gasification in 15% CO_2 at 850°C, 900°C, and 950°C. Temperature profiles are included in the panels (red, blue, and green dashed lines). CO_2 is injected at the times indicated by the black dotted lines.

Figure 4.3 shows the effects of CO_2 concentration on char gasification and alkali release. The pyrolysis stage is included on the left-hand side of the dotted line and shows high-level reproducibility. A higher CO_2 concentration increases the probability that CO_2 reaches the active sites on the char surface, producing a higher gasification rate. For char gasification with high CO_2 concentrations, the release of alkali increases slightly due to the high gasification rate.

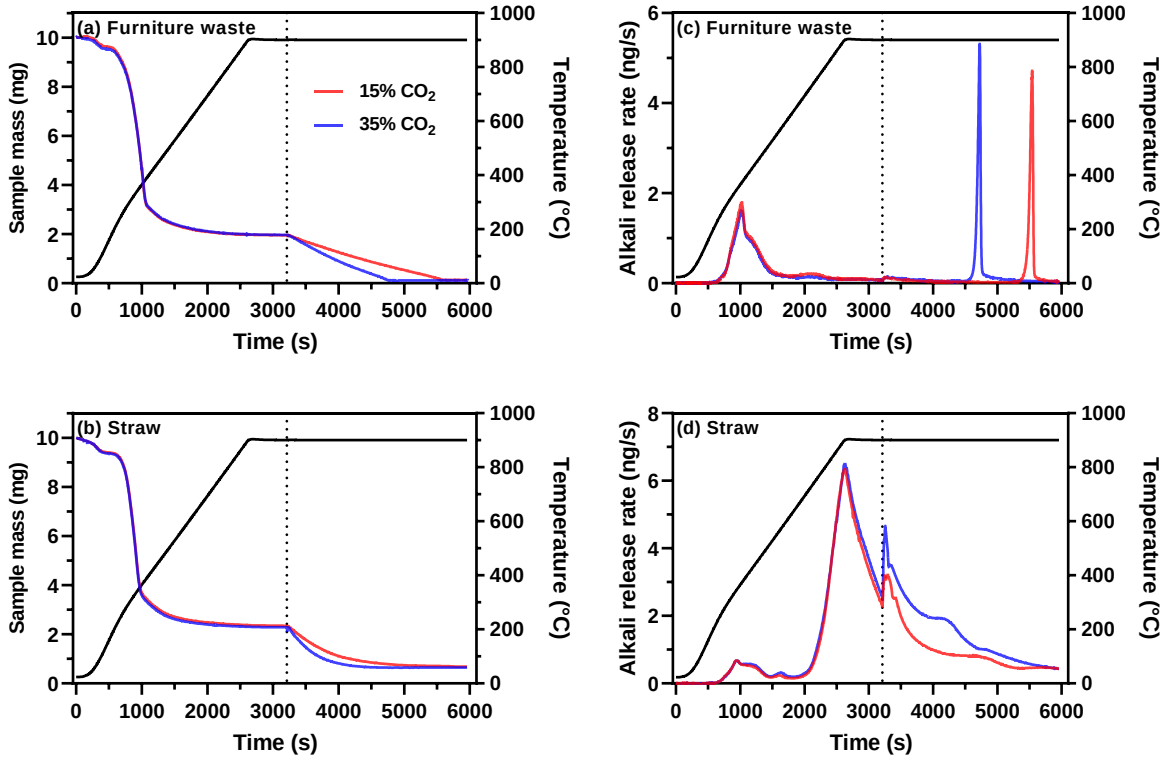

Figure 4.3 (a, b) Sample mass and (c, d) alkali release during heating in N_2 and isothermal gasification in CO_2 of furniture waste and straw. The solid black line represents the temperature profile. CO_2 is injected at the time indicated by the black dotted line.

4.1.3 Effect of alkali content in chars

In this subsection, the feedstocks referred to are the industrial chars shown in Table 3.2. Figure 4.4 shows the alkali release dynamics during heating of the chars with different alkali contents from room temperature to 900°C. Only the KCl-added char shows clear alkali release starting from 700°C. The starting release temperature is close to the temperature at which pure KCl starts to vaporize. However, the other chars do not exhibit alkali release, and this is attributed to the high temperature in the industrial process. The industrial gasifier has an operating temperature of up to 1100°C [120], which is likely to result in extensive release of alkali, which explains the lack of releasable alkali at 900°C. This result shows that the intrinsic alkali in the original char is more difficult to release than the additional added KCl.

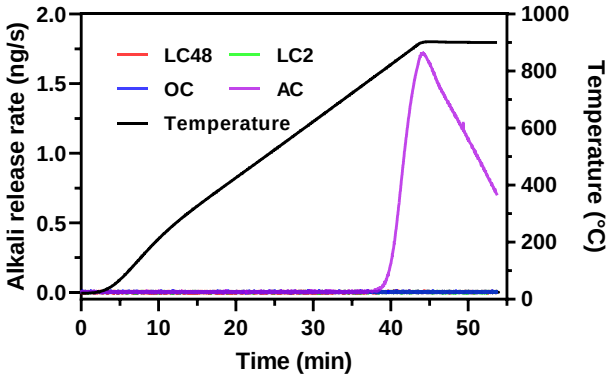

Figure 4.4 Alkali release as a function of time during heating from 25°C to 900°C in N_2 for the samples with different alkali contents. The following samples were used in the experiments: original char (OC); OC leached for 2 h (LC2); OC leached for 48 h (LC48); and KCl-added char (AC). A temperature profile is included in the panel.

Figure 4.5a shows the gasification reactivities of the chars with different alkali contents. For the original and leached chars, the gasification reactivity of the whole process increases with increasing alkali content. In contrast, the reactivity of KCl-added char (AC) does not increase at $X<0.6$ compared to the OC, while it increases significantly as conversion proceeds above $X=0.6$. The alkali release behavior differs substantially between the non-KCl-added chars and the KCl-added char, i.e., the three non-KCl-added chars do not release any alkali before the gasification approaches completion ($X<0.8$). Alkali release from the KCl-added char increases rapidly when the gas is switched to the CO_2 and N_2 mixture, which is attributed to the oxidizing atmosphere enhancing alkali release [114,115]. The alkali release rapidly decreases at $X<0.1$, then gradually decreases until $X=0.8$, after which the alkali release again increases and shows a remarkable level of alkali release in the final stage of gasification. The OC and LC2 show significant levels of alkali release when char gasification approaches completion, and the release rate decreases with a decrease in the alkali content of the char. However, the LC48 does not release alkali at a significant level throughout the gasification process. The observed release of alkali when the gasification approaches completion seems to correspond to the conversion rate of char, i.e., the char with obvious alkali release always manifests an increase in the char conversion rate. The LC48 sample neither releases alkali nor shows an increase in conversion rate during the final gasification stage.

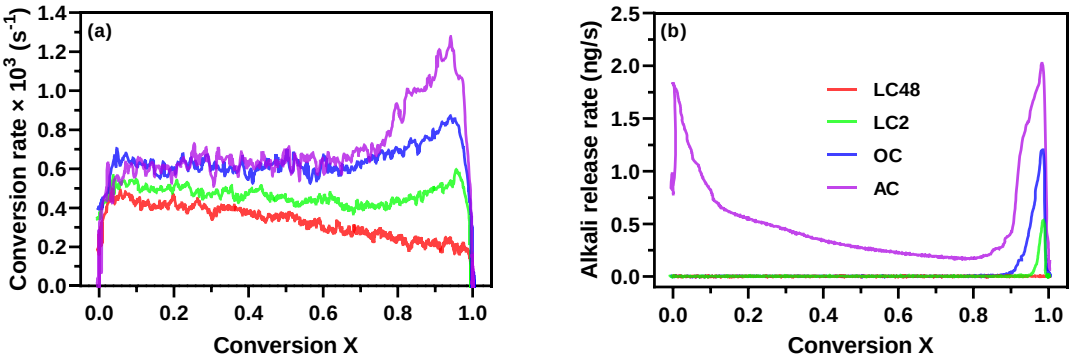

Figure 4.5 (a) Conversion rate *r* and (b) alkali release rate as a function of conversion X during the gasification of chars with different alkali contents at 875. The following samples were used in the experiments: original char leached for 48 h (LC48); original char leached for 2 h (LC2); original char (OC); and KCl-added char (AC).

4.2 Co-pyrolysis and co-gasification of wood and straw

Co-gasification is a technology for efficient thermal conversion of fuels. It is well-known that some of the synergistic effects that occur during co-gasification are due to alkali migration from an alkali-rich fuel to an alkali-deficient fuel [15,16]. Previous studies have often used one alkali-rich biomass to promote the pyrolysis and gasification of fossil fuels. However, due to the limited resolution of offline alkali measurements, these studies have not provided sufficient information regarding the migration of alkali between two types of fuel. Two types of biomass with significantly different alkali contents were used here, i.e., wood and straw, to investigate alkali migration and synergistic effects during co-conversion using the setup shown in Figure 3.1. Wood and straw show totally different alkali release profiles during their char gasification (Section 4.1), and it is interesting to study the levels of alkali release during the gasification of wood and straw mixtures. Details can be found in **Paper II**.

4.2.1 Co-pyrolysis of wood and straw

Figure 4.6 shows the mass and alkali results for the pyrolysis of pure wood, pure straw, and a mixture of 75% wood and 25% straw (WS75). The calculated mass ratio and calculated mass loss rate for WS75 are based on a linear combination of the corresponding values for pure wood and pure straw [Equation (4)]. The calculated mass results largely overlap with the experimental mass results for WS75, as shown in Figure 4.6, a and b. This suggests that there are no synergistic effects from the perspective of sample mass loss during pyrolysis. The result is discrepant with the results of previous studies on the co-pyrolysis of biomass and fossil fuels, in which a positive synergistic effect was observed for the mass loss in a process conducted at a temperature above 400°C [17,18]. The reason for this discrepancy may be that wood and straw have similar structures and release volatile matter mainly at temperatures below 400°C [132], whereas fossil fuels have different structures than biomass and tend to release more volatile matter at temperatures above 400°C. Thus, the inorganic

elements in biomass can catalyze the decomposition of heavy volatile matter in fossil fuels, resulting in a synergistic effect on the mass loss.

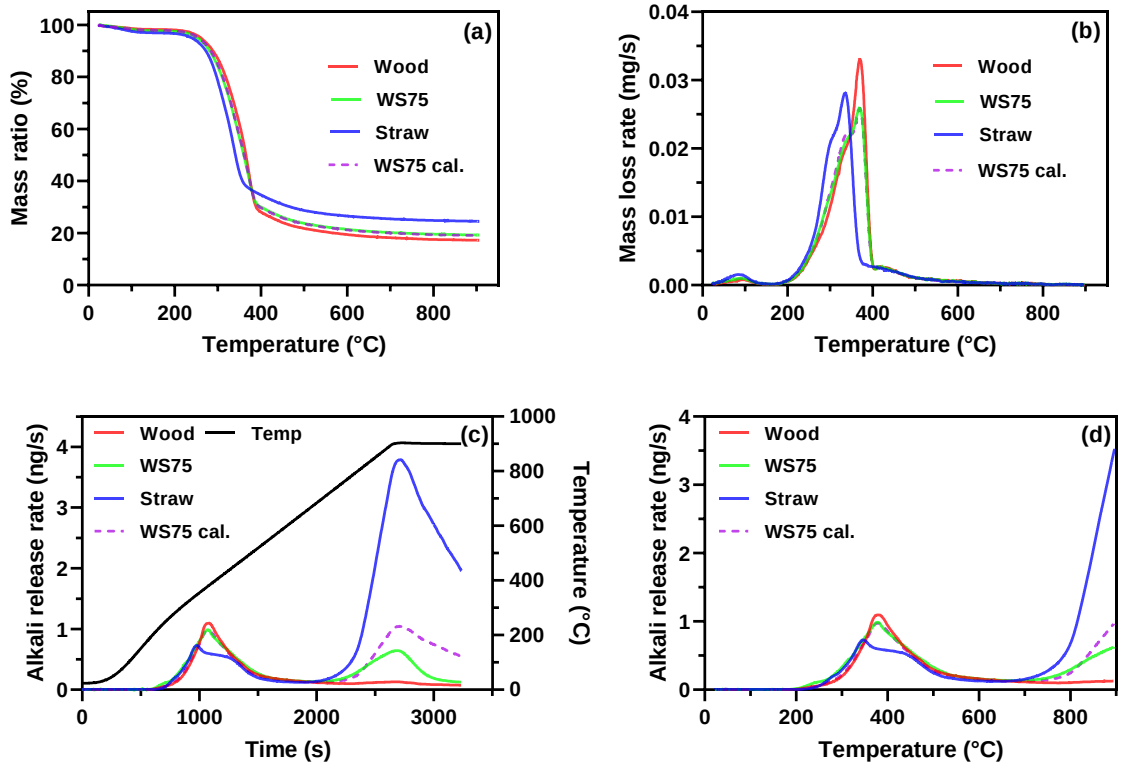

Figure 4.6 (a) Mass ratio, (b) mass loss rate, and (d) alkali release rate as a function of temperature during pyrolysis. (c) Alkali release rate and temperature as a function of time during pyrolysis. Samples include wood, a mixture with 75% wood (WS75), and straw. Calculated values (WS75 cal.) based on a linear combination of the results for pure wood and straw are included for comparison (dashed lines).

The calculated alkali release curves in Figure 4.6, c and d are based on a linear combination of the results for pure wood and straw samples [Equation (5)]. The experimental and calculated curves for the mixture with 75% wood overlap when the process temperature is lower than 800°C. This indicates that the amount of alkali released from the mixture is proportional to the ratios of alkali released from the two original materials, so no synergistic effect is observed. However, when the temperature is >800°C, the experimentally observed alkali release is lower than the calculated curve, and the difference becomes more significant with increasing temperature. This indicates the migration of alkali from the straw to the wood. Alkali that is released to the gas phase from the straw may be adsorbed by the char surface owing to the large surface area and low alkali content of the wood char. The migration of alkali may also take place through the transfer of alkali-containing melts. Low-melting-point alkali melts on the straw char surface [133,134], e.g., alkali silicates, adhere to the wood char surface.

4.2.2 Co-gasification of wood and straw

Figure 4.7 shows the conversion process and alkali release during co-gasification of wood and straw with various blend ratios. The calculated values are calculated using the same linear combination of pure wood and straw results as in Section 4.2.1. Figure 4.7a shows that the experimental co-gasification processes take less time than the calculated time to reach the same level of conversion. This indicates the synergistic effect that occurs during the co-gasification of wood char and straw char. To investigate the detailed synergistic effect for different conversion processes, Figure 4.7, b and c show the conversion rate as a function of the conversion X during co-gasification for mixtures with different blend ratios. The conversion rates of the experimental curves are higher than those of the calculated curves for the same conversion during most of the gasification stage. The positive synergistic effect seen during most of the gasification stage is attributed to the alkali migration mentioned in Section 4.2.1, and is supported by the SEM-EDS results in **Paper II**. The conversion rates of the experimental curves are lower than those of calculated curves when the gasification approaches completion, which indicates a negative synergistic effect. The negative synergistic effect is attributed to silicon migration from the straw to the wood via the gas phase [135] or, alternatively, through the transfer of silicate melts [133,134]. The SEM-EDS results in **Paper II** further show that the wood char surface in mixtures with 90% wood has a much higher silicon content than the pure wood char surface after gasification for 5 min. The synergy index was calculated to evaluate the synergistic effects of the different mixtures at various conversions. The mixture with 75% wood showed the highest synergy index, as shown in Figure 4.7d. The highest synergistic effect is attributed to the sufficiently high wood content and the sufficient supply of alkali at this mixing ratio.

The experimental results for alkali release during gasification of the samples with different mixing ratios are shown in Figure 4.7e. Since alkali release is affected by the char conversion rate, it is difficult to compare the experimental and calculated alkali release profiles. The alkali release during most of the gasification stage correlates with the straw content, i.e., a high straw content result in a high level of alkali release. The main finding here is that even a low content of straw can reduce or eliminate the remarkable alkali release seen in the final stage of wood gasification. This effect is attributed to silicon that migrates from the straw surface to the wood surface and combines with alkali to form non-releasable alkali silicates [21,126,136–140]. In addition, other elements that show significant migration (see **Paper II**), e.g., Al and P, may play roles similar to that of silicon.

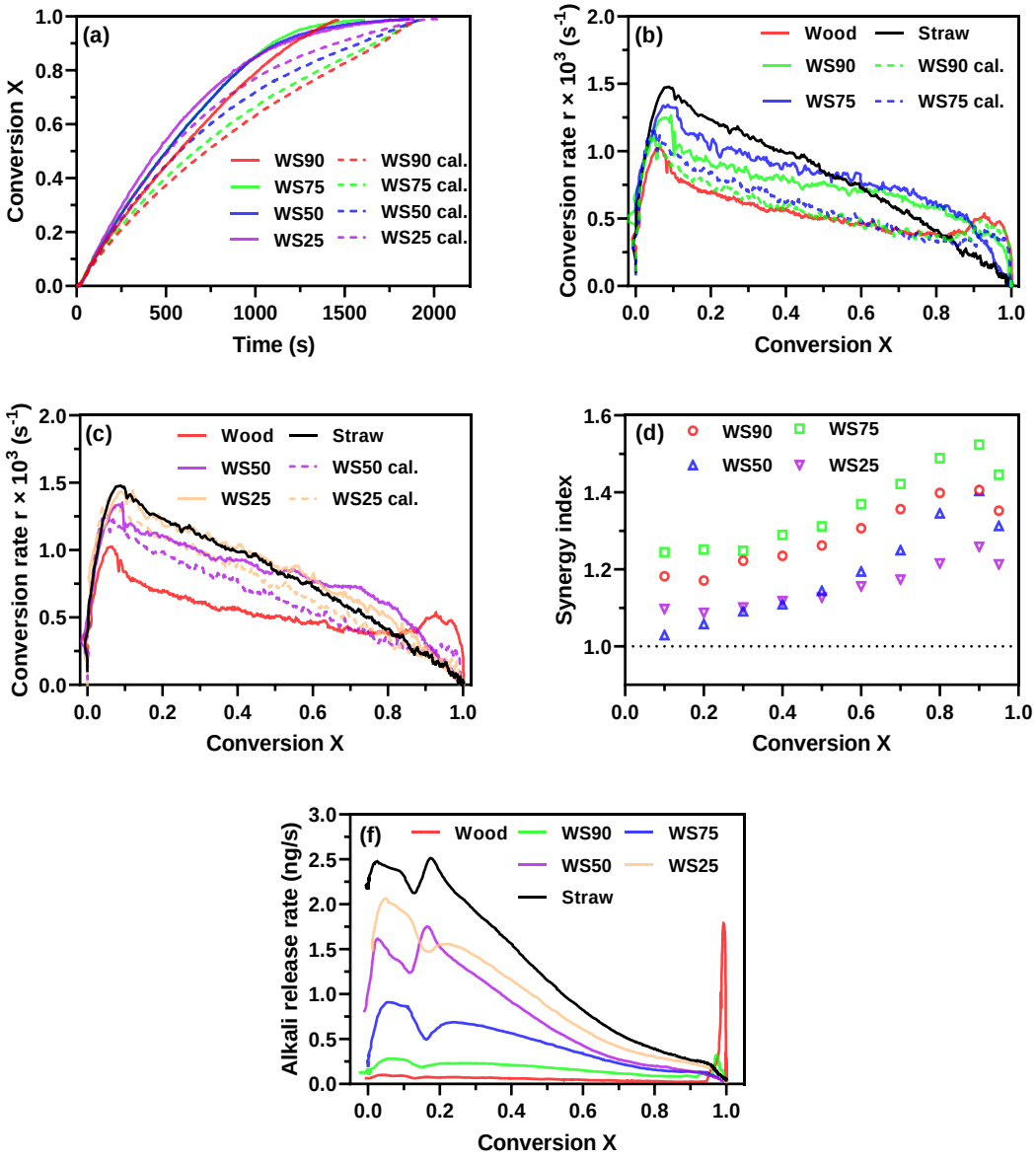

Figure 4.7 (a) Conversion as a function of time, and (b, c) conversion rate, (d) synergy index, and (e) alkali release rate as a function of conversion during the gasification of wood, straw, and mixtures with 25%–90% wood (e.g., WS25). Calculated values (e.g., WS25 cal.) based on a linear combination of the results for pure wood and straw are included for comparison (dashed lines).

4.3 Effects of fresh bed materials on biomass gasification

Fluidized bed materials promote efficient heat transfer and catalytic functions in the thermochemical conversion of biomass. This section described the investigations of the effects of six commonly used bed materials on wood and straw pyrolysis and their char gasification, with the emphasis on alkali release and reaction perspectives. The six bed materials used were silica, sea sand, olivine, ilmenite, alumina and dolomite. Their elemental analyses are shown in Table 3.3. Section 4.3.1 presents the effect of bed material on wood char gasification (see the pyrolysis results and other details regarding gasification in **Paper III**). Section 4.3.2 describes the results for the

effects of the bed materials on straw char gasification (for additional details, see **Paper IV**).

4.3.1 Effects of fresh bed materials on wood gasification

Figure 4.8, a and c depict the effects of the six bed materials on char gasification processes using bed material masses of 1 mg and 10 mg, respectively. All the bed materials affect wood char gasification, and the effect is significantly different for different bed materials. At low levels of conversion, silica (X<0.5), olivine (X<0.7) and ilmenite (X<0.7) have no effects on char gasification reactivity. In contrast, at low levels of conversion, sea sand (X<0.8), alumina (X<0.8), and dolomite (X<0.7) promote char gasification, and this is related to alkali migration from the bed materials; in the case of dolomite, it also involves the conversion of carbon deposits formed during pyrolysis. Table 4.1 clearly shows that the wood char surfaces derived from the mixtures of wood and sea sand and of wood and alumina have higher sodium contents than the pure wood char. The sodium should be from the corresponding bed material in the mixtures, due to the high sodium contents of sea sand and alumina, as shown in Table 3.3. The high reactivity seen for the char from the wood and dolomite mixture is due to the gasification on the dolomite surface of the deposits that formed during pyrolysis (see the pyrolysis results in **Paper III**). When the gasification approaches completion, the silicon-rich bed materials, i.e., silica, sea sand, olivine, and dolomite, reduce the gasification reactivity of the wood char, and this is related to silicon migration from the bed material to the wood char surface. Table 4.1 also shows a higher silicon content on the char surface for the samples that contain a silicon-rich bed material. The migrated silicon can react chemically with the alkali to form catalytically inactive silicates [96], with the result that the reactivity is reduced. The addition of ilmenite has an effect similar to that of the silicon-rich bed materials, which is attributed to a reaction that occurs between titanium compounds and alkali [141].

With respect to the release of alkali, most of the samples have low and similar alkali release rates before the char gasification approaches completion, although dolomite promotes higher release, as shown in Figure 4.8, b and d. The high level of alkali release observed for the dolomite addition case is attributed to the migration of Mg and Ca from the dolomite to the char (Table 4.1). The migrated Mg^{2+} and Ca^{2+} combine preferentially with aluminosilicate compounds, which allows more potassium to survive in releasable forms [29,100,142–144]. When the char gasification approaches completion, alkali release is largely inhibited after mixing with the bed materials. The peak level of alkali release almost disappears when 10 mg of silica, sea sand, olivine, ilmenite, or dolomite are added (Figure 4.8d). The reason for this is that alkali on the char surface combines with migrated Si or Ti, as discussed in the last paragraph. The reduction of alkali release after alumina addition is possibly due to the bed material being able to absorb some of the alkali [105,145].

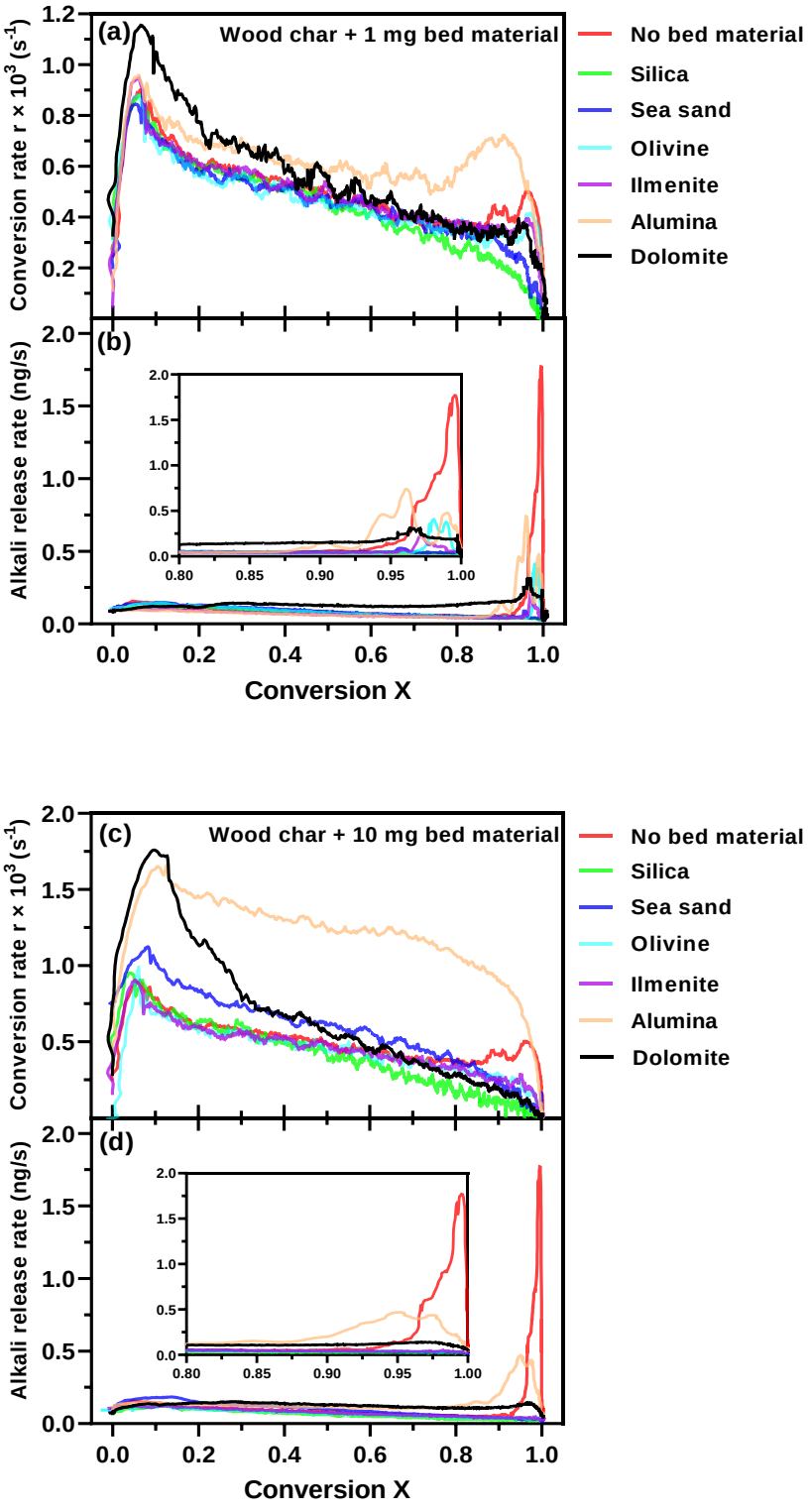

Figure 4.8 (a, c) Char conversion rate *r* and (b, d) alkali release rate as a function of char conversion X during the gasification of wood char (approximate 1.6 mg) mixed with 1 mg or 10 mg of bed material. Insets display the data during the final conversion stage in greater detail.

Table 4.1 Average relative mineral contents on the char surface, as measured by SEM-EDS, for a conversion X value of 30%. The samples initially contained 10 mg of wood and 10 mg of the indicated bed materials.

Bed material	No bed material	Silica	Sea sand	Olivine	Ilmenite	Alumina	Dolomite
Mineral matter (atomic conc.)							
Mg	23.04	6.42	12.92	40.80	13.35	7.86	37.92
Ca	51.79	36.95	35.59	25.57	53.16	40.39	33.86
K	12.55	7.63	13.28	9.91	11.60	6.65	14.29
Si	3.02	40.02	20.24	14.08	2.04	0.25	9.00
Fe	4.68	1.72	4.93	5.55	7.13	1.41	2.22
Na	1.99	5.92	12.37	2.04	1.52	15.67	1.12
Al	2.34	1.34	0.67	1.38	1.21	27.78	1.08
Ti	0.59	0	0	0.69	9.75	0.00	0.52

4.3.2 Effects of fresh bed materials on straw gasification

The conversion rates during gasification of straw char with the addition of 10 mg of the different fresh bed materials are shown in Figure 4.9a. The addition of dolomite increases the char conversion rate during the initial stage ($X<0.3$), which is attributed to the high reactivity of the carbon deposits formed on the dolomite surface during the pyrolysis stage. However, the char reactivity seems lower than that of the pure straw char during the remainder of the process ($X>0.3$), which may be due to a high level of alkali loss (discussed in the following paragraph). Silicon- or titanium-containing bed materials tend to reduce the char gasification reactivity with the following relative degree of reduction, in order of high to low: silica > ilmenite > olivine ≈ sea sand. It should be noted that the char reactivities in the cases of olivine and sea sand are very similar to that of the pure straw char, although they show a clear inhibitory effect when more bed material is added (see details in **Paper IV**). The SEM-EDS results listed in Table 4.2 reveal an increase in silicon or titanium on the straw char surface following the addition of the four silicon- or titanium-containing bed materials. The migrated silicon or titanium may react chemically with alkali to form catalytic inactive compounds [96,141], thereby reducing the char reactivity, as discussed in Section 4.3.1. The addition of alumina significantly reduces the char gasification reactivity, which is much different from the effect of alumina seen during wood char gasification (Section 4.3.1). As shown in Table 4.2, aluminum was observed to migrate from the alumina to the straw, and the pure straw char surface has a silicon content >55%. In addition, the SEM-EDS results in Figure 4.10 show that the outer layer of the straw char particles forms a shell with a high silicon content. Therefore, the migrated aluminum can react chemically with K, Ca, and Si, which are abundant on the surface of the straw, to form complex K-Al-Si (e.g., $KAlSiO_4$, $KAlSi_2O_6$, and $KAlSi_3O_8$) and Ca-Al-Si (e.g., $Ca_2Al_2SiO_7$ and $CaAl_2Si_2O_8$) compounds, respectively [138–140]. The formed ternary compounds lack catalytic activity, resulting in the inhibition of char gasification.

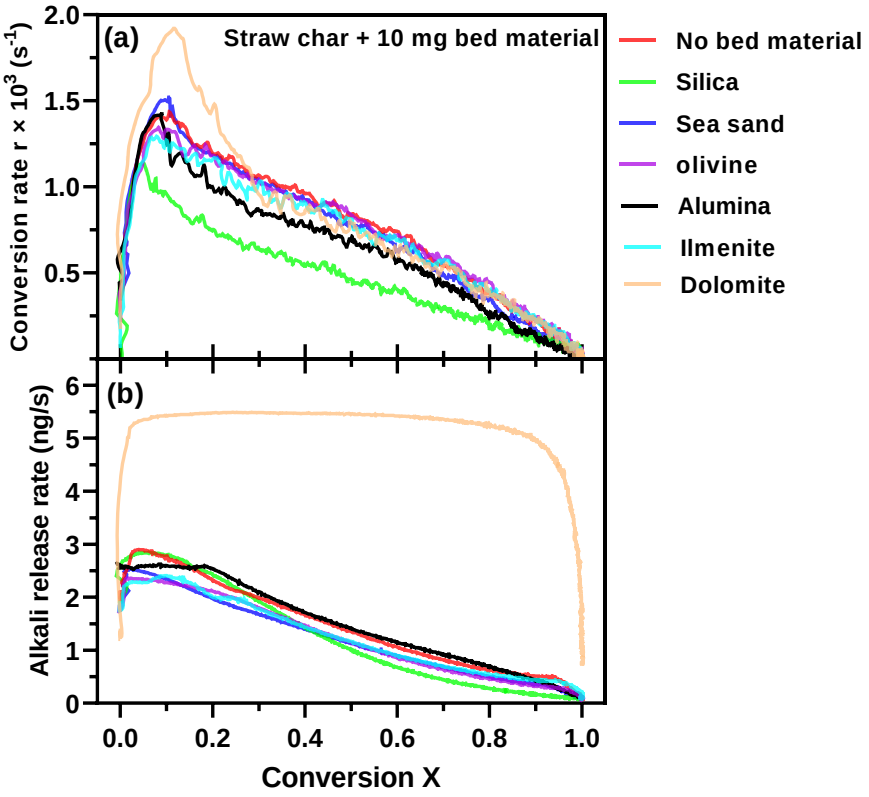

Figure 4.9 (a) Char conversion rate *r*; and (b) alkali release rate as a function of char conversion X during the gasification of wood char mixed with 10 mg of bed material.

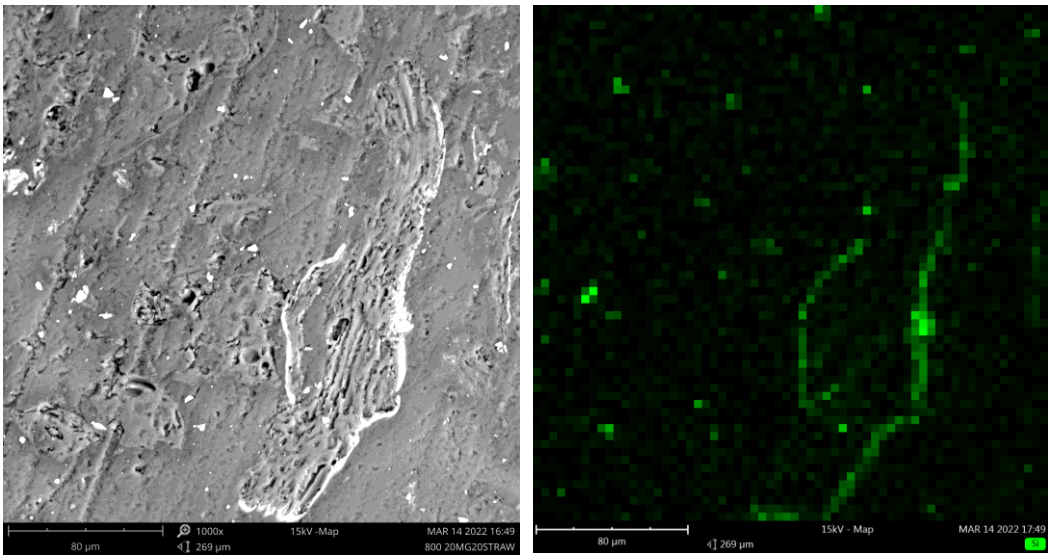

Figure 4.10 (a) Morphology and (b) silicon distribution of a cross-section of a straw particle, as measured by SEM-EDS.

Figure 4.9b shows the alkali release profiles during the gasification of straw char with the addition of 10 mg of the different bed materials. The addition of dolomite significantly enhances alkali release during straw char gasification, which is attributed

to the migrated Mg^+ and Ca^+ preferably combining with silicates, so as to allow more K to survive in releasable forms [29,100,142–144]. The significant alkali release seen after dolomite addition results in a high level of alkali loss, which may be the reason for the decrease in char reactivity. Although the addition of alumina inhibits straw char gasification, the rate of alkali release during the gasification does not seem to decrease significantly. The reasons for this may be that the high sodium content of the alumina compensates the alkali release via a complex process, and that the ternary K-Al-Si melts release some alkali. Other bed materials, i.e., silica, sea sand, olivine, and ilmenite, reduce the level of alkali release during char gasification to different extents, possibly due to alkali combining with the migrated silicon or titanium. In addition, the possibility that some alkali is adsorbed by the bed materials cannot be excluded.

Table 4.2 Average mineral concentrations on the char surface measured by SEM-EDS at a conversion X of 30%. The samples initially contained 10 mg of straw and 10 mg of the indicated bed materials.

Bed material	No bed material	Silica	Sea sand	Olivine	Ilmenite	Alumina	Dolomite
Mineral matter (atomic conc.)							
Si	62.54	75.41	71.22	39.03	60.7	55.01	26.72
K	24.65	11.86	10.89	14.31	20.02	21.17	14.05
Ca	9.27	3.79	4.62	5.86	5.64	5.01	33.63
Na	0	6.4	6.74	4.99	0	1.57	1
Mg	1.71	0.68	3.13	1.65	12.45	3.15	23.72
Ti	0.29	0	0	0	0	6.64	0.59
Fe	1.54	1.87	1.35	0	0.62	7.17	0
Al	0	0	1.45	34.17	0.58	0.32	0

4.4 Effects of used bed materials on char gasification

Extensive studies have shown that an ash layer is usually formed on the bed material particles after the biomass thermal conversion processes are operated for a few days in fluidized beds [27–33]. The formed ash layer is rich in AAEMs, which are commonly found in biomass [99]. The AAEM-coated bed material may release some elements during the high-temperature process, and these may exert catalytic effects on the process [34,102–104,106,107]. The used bed materials applied in this study were collected from a BFB boiler and a CFB boiler, and the samples had experienced different numbers of days in the boilers (for details regarding the bed materials, see Section 3.1.4). Alkali release from the used bed materials, alkali migration from the bed material to char, and the effects of the used bed materials on char gasification were studied. The detailed results are included in **Paper V**.

4.4.1 Alkali migration from bed material to char

Alkali release from the original industrial char (OC), used bed materials, and mixtures thereof with different blend ratios are shown in Figure 4.11. The OC does not release alkali during heating from room temperature to 950°C, which is explained by the extensive release of alkali in the entrained-flow gasifier where the

char already experienced temperatures of up to 1100°C [120]. In contrast, all the used bed materials release alkali, and the rate of alkali release increases with the number of the days that the bed material remains in the fluidized bed. Earlier studies of the same bed materials as used here have shown that the thickness of the coating layer increases with the number of the days that the bed material resides in the fluidized bed, and that the coating layers are rich in AAEMs, i.e., Ca and K [30,31,36,100]. Therefore, a bed material that experiences more days in a fluidized bed has a higher alkali content and may, as a consequence, release more alkali. In addition, alkali release starts at 820°C, increases as the temperature rises until the maximum temperature of 950°C, and decays thereafter during the isothermal stage at 950°C. The levels of alkali release from the mixtures of industrial char and used bed materials are generally lower than the sum of the levels of alkali release from the two individual materials, which indicates that there is gas-phase alkali migration from the bed material to the char. In addition, other elements, including Mg, Ca and Si, are observed to migrate from the bed materials to the char, as revealed by SEM-EDS (**Paper V**). The migration mechanisms may include both gas-phase migration and transfer of melted phases through direct contact between the materials [30,133,134,146–148].

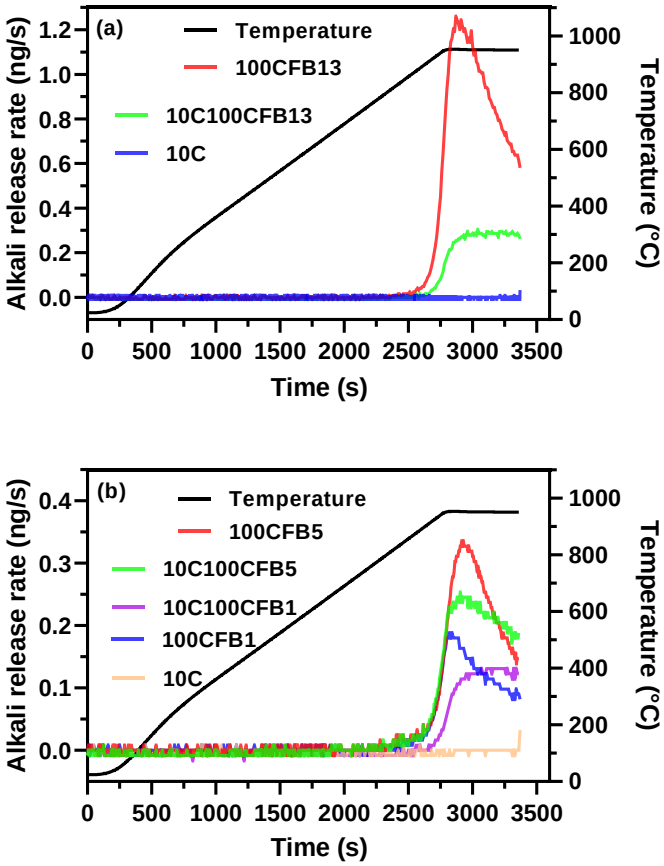

Figure 4.11 (a) Alkali release from 10 mg of char (10C), 100CFB13, and a mixture of 10C and 100CFB13 (10C100CFB13) during heating in N_2; (b) alkali release from 10C, 100CFB1, 100CFB5, 10C100CFB1, and 10C100CFB5 during heating in N_2. As an example to explain the sample naming system: 100CFB13 corresponds to 100 mg of circulating fluidized bed material with operational time of 13 days.

4.4.2 Effects of used bed material on char gasification and alkali release

The effects of used bed material on char conversion and alkali release during isothermal gasification are shown in Figure 4.12. A bed material that had experienced 13 days in a circulating fluidized bed (CFB13) was selected for the study because it has the thickest ash coating layer [36] and the highest level of alkali release (Section 4.4.1) of the investigated samples. The addition of 4 mg of bed material to 10 mg of char changes the entire char gasification process compared to using pure char. As more bed material is added, char gasification is enhanced during the initial stage or most of the gasification stage. The increase in reactivity is attributed to the catalytic effects of the migrated elements, i.e., K, Ca and Mg, which originate from the bed material [60,62,120,128,130,143,149]. Note that char reactivity does not appear to increase significantly when the amount of bed material is increased from 20 mg to 100 mg for $X<0.5$, indicating catalytic element saturation on the char surface. The reduced reactivity observed during the final stage or last moments of char gasification is attributed to silicon migration from the bed material to the char surface. Silicon, which is the most-abundant element in the used bed material, is observed to migrate from the bed material to the char surface, as revealed by SEM-EDS (**Paper V**). Therefore, as more bed material is added, more silicon migrates from the bed material to the char surface, inducing a greater reduction of reactivity. Similar results were obtained in the study of co-conversion and fresh bed material in Sections 4.2 and 4.3.

The level of alkali release is higher for the mixture that has more bed material added, except for during the stage when the gasification approaches completion, as shown in Figure 4.12b. Alkali release from the individual used bed material always decays during isothermal heating (**Paper V)**, while alkali release from the mixtures increases as char conversion proceeds. This enhancement of alkali release may be attributed to the migration of Ca and Mg. Some previous studies have shown that Ca and Mg preferably combine with silicates, thereby ensuring that more alkali survives in releasable form [29,100,142–144]. When the char gasification approaches completion, the pure char releases alkali. However, the pronounced alkali release decreases with the addition of used bed material, probably due to the chemical reactions that occur between alkali and the migrated silicon [54,108,137].

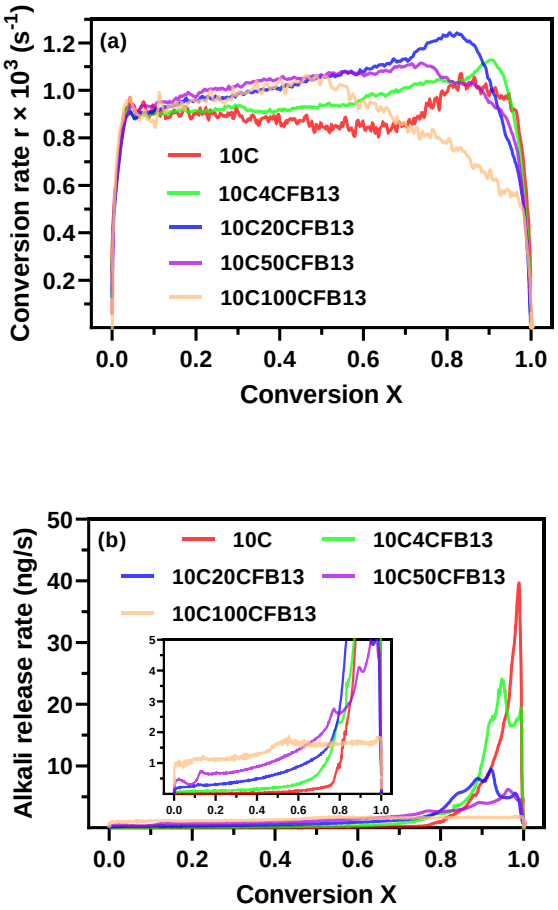

Figure 4.12 (a) Conversion rate *r* and (b) alkali release rate as a function of conversion X during CO_2 gasification of industrial char with or without bed material addition. The bed materials have various masses, although they have spent the same number of days in a fluidized bed.

4.4.3 Effects of the bed material operating days on char gasification

The number of days that a bed material has participated in the industrial process influences the char gasification reactivity, as illustrated in Figure 4.13. The bed material that has experienced only 1 day in the CFB does not show any catalytic effects at low conversions (X<0.7), while bed materials that have been used for 5 days or 13 days significantly increase the char gasification reactivity. The catalytic effect is attributed to the migration of AAEMs from the coating layer of the used bed materials to the industrial char [60–62,120,128,130,143,144,146,149–152]. The coating layer grows and develops with time in the boiler. The layer formed after 1 day in the CFB is still thin and contains limited amounts of catalytic elements [31,36], such that the effect on char reactivity is marginal. After 5 days and 13 days in the CFB, the layer has developed significantly and the effect on char reactivity is pronounced. The results after 5 day and 13 days at X<0.5 are similar, which may reflect a saturation effect of the catalytic elements. All three bed materials reduce the char reactivity at conversions above X=0.7, due to the migration of silicon from the bed material to the char. This is similar to the effect that Si-containing fresh bed materials have on

reducing char gasification (see Section 4.3). The alkali release for X<0.7 increases with the number of the days that the bed material spends in the CFB. The reason for the increase in alkali release at X<0.7 is that a bed material that has spent more days in the CFB releases more alkali (Figure 4.11) and contains more alkaline earth metals, e.g., Mg and Ca, which can react with silicate to ensure that more alkali survives in releasable forms, as is also observed for the addition of dolomite to wood and straw (Section 4.3) [29,100,142–144]. At X>0.7, the rate of alkali release decreases dramatically after the addition of CFB materials, as compared to the pure industrial char. More days spent in the CFB seem to result in a more-pronounce significant reduction in alkali release, which may be associated with an increased amounts of silicon on the char surface [61,128].

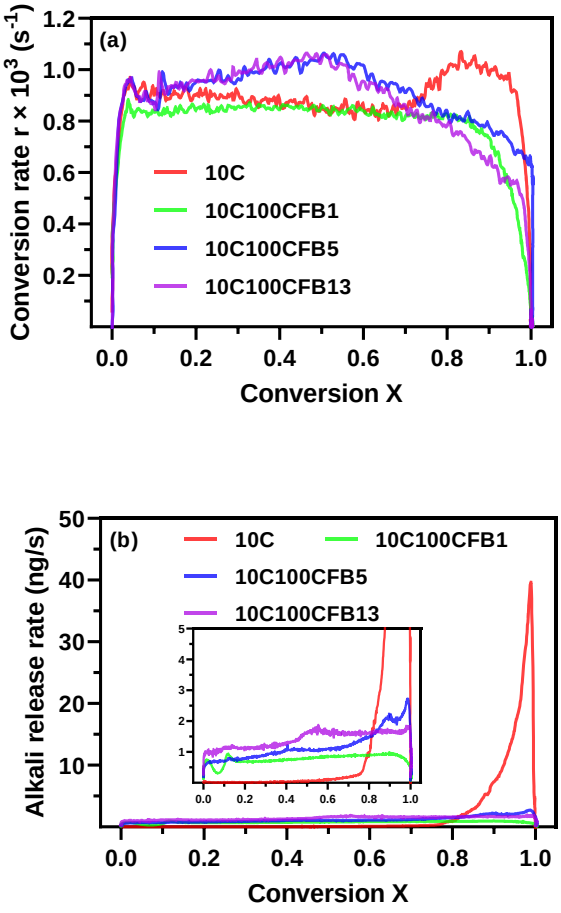

Figure 4.13 (a) Conversion rate *r* and (b) alkali release rate as a function of conversion *X* during CO_2 gasification of 10 mg of industrial char, and mixtures of 10 mg char and 100 mg of CFB material. The bed materials have experienced 1, 5 or 13 operational days in the industrial process.

4.5 Alkali and particle release during steam gasification of char

Steam gasification is an approach that is used to convert fuel into H_2-rich syngas [153]. This section describes the usage of the original industrial gasifier char (OC), furniture waste char, and straw char as feedstocks to investigate the alkali and particle release profiles during steam gasification at 850–950°C. The setup used in the study is the fixed bed system shown in Figure 3.3. To exclude the effects of bed material, no bed material was added to the fixed bed.

4.5.1 Alkali release during gasification of biochar

Figure 4.14 shows the results of the online measurements of alkali release during steam gasification of the industrial gasifier char (OC) at temperatures ranging from 850°C to 950°C. Before steam injection, low concentrations of CO, CO_2 and alkali were observed, which are associated with the release of volatiles remaining in the char. The temperature was stabilized at the selected gasification temperature (850–950°C) for 10–20 mins, after which steam was introduced into the reactor to initiate gasification. When the steam was injected into the reactor, the levels of CO and CO_2 immediately increased to more than 1500 ppm, although they quickly dropped to hundreds of ppm and continued to decrease until the final gasification stage. During this stage, the levels of CO and CO_2 increased again for a short time and rapidly dropped to a low level as the conversion finished. The renewed increases of CO and CO_2 are related to the gasification reactivity increase in the final stage of woody char gasification, caused by the catalytic effects of alkali [154]. Similar results were observed in the study of CO_2 gasification (Section 4.1). A higher temperature shortened the time required for the gasification process, which indicates a higher gasification reactivity.

Regarding alkali release, it increased gradually until the end of the char gasification, at which point it reached its maximum value. This may be due to gradual alkali enrichment of the char during the gasification [61], resulting in a high level of alkali release at high conversions. The process of alkali release in steam is different from that of CO_2 char gasification (Figure 4.5), since the latter only shows minor alkali release, except for the stage in which the char conversion approaches completion. This difference may be attributable to the gasifying agent. Steam causes some alkali to combine with OH^- to form KOH, which has a relatively high vapor pressure [155]. In contrast, CO_2 may cause alkali elements to convert to carbonates, which are difficult to release at these gasification temperatures [70,156].

In addition, a high temperature resulted in high gasification reactivity, as indicated by the CO and CO_2 curves in Figure 4.14. At the same time, a more-pronounced alkali release was observed at high temperatures. The high alkali concentration may be due to the high mass loss rate that occurs at high temperatures and the fact that a high temperature promotes alkali release [157].

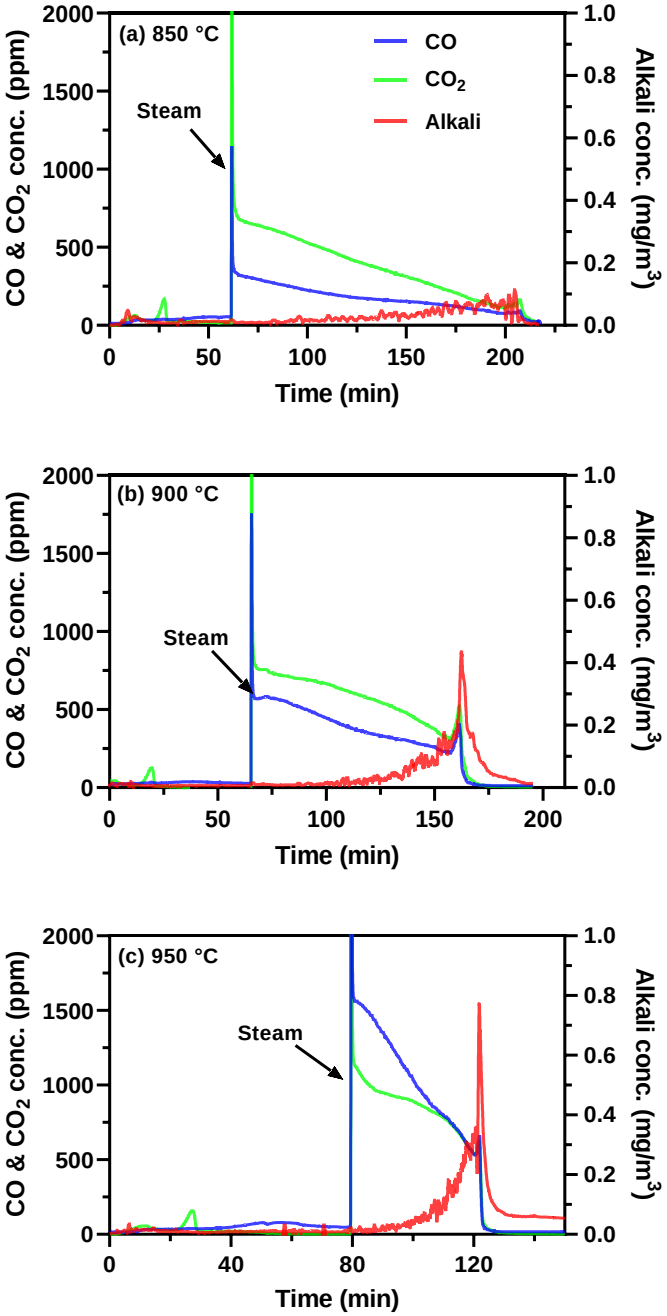

Figure 4.14 CO, CO_2, and alkali concentrations during isothermal gasification of original char at: (a) 850°C; (b) 900°C; and (c) 950°C. The black arrows indicate the time of steam injection (a few seconds before the CO and CO_2 concentrations start to increase). The char was heated in N_2 from room temperature to the designed gasification temperature before steam injection.

4.5.2 Particle release during gasification of biochar

The pattern of particle release during the gasification of industrial gasifier char is shown in Figure 4.15. The particles may be formed through the nucleation of condensable material when the flow from the reactor is cooled or the fly ash and unconverted char is transported away from the reactor by the flow. Particles in two size ranges are measured: Small particles (10.7– 478 nm) are measured using SMPS; and large particles (575–8,750 nm) are measured using OPS. The particle total mass concentrations of the two size ranges gradually increase during the char gasification, as shown in Figure 4.15. The particle release trend is quite similar to the alkali release pattern, which is reasonable as the alkali is also in the particle phase after exiting the reactor.

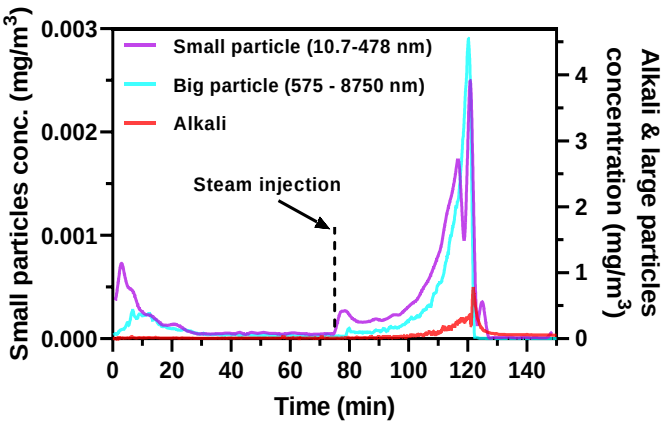

Figure 4.15 Alkali, small particles (10.7–478 nm), and large particles (575–8,750 nm) concentrations during char gasification at 950°C. The dashed line indicates the time when the isothermal char gasification starts.

4.5.3 Comparison of the gasification processes for different chars

The CO, CO_2, and alkali concentrations during isothermal steam gasification of industrial char, furniture waste char, and straw char are shown in Figure 4.16. The furniture waste char and straw char were produced by pyrolysis of the corresponding biomasses (Table 3.1) in a fixed bed for 2 h in an N_2 atmosphere. The generated chars were sieved to the same size range as the OC. The gasification steps were the same as those for the steam gasification of the OC.

During the heating stage, all three chars emit some CO and CO_2, which is related to some unconverted tars and volatiles. Industrial char and furniture waste char release insignificant amounts of alkali in this stage. In contrast, straw char shows a major alkali release from 25 to 70 min, where the temperature is estimated to be in the range of 600–900°C. The maximum level of alkali release during heating of the straw char is reached at the maximum temperature (900°C).

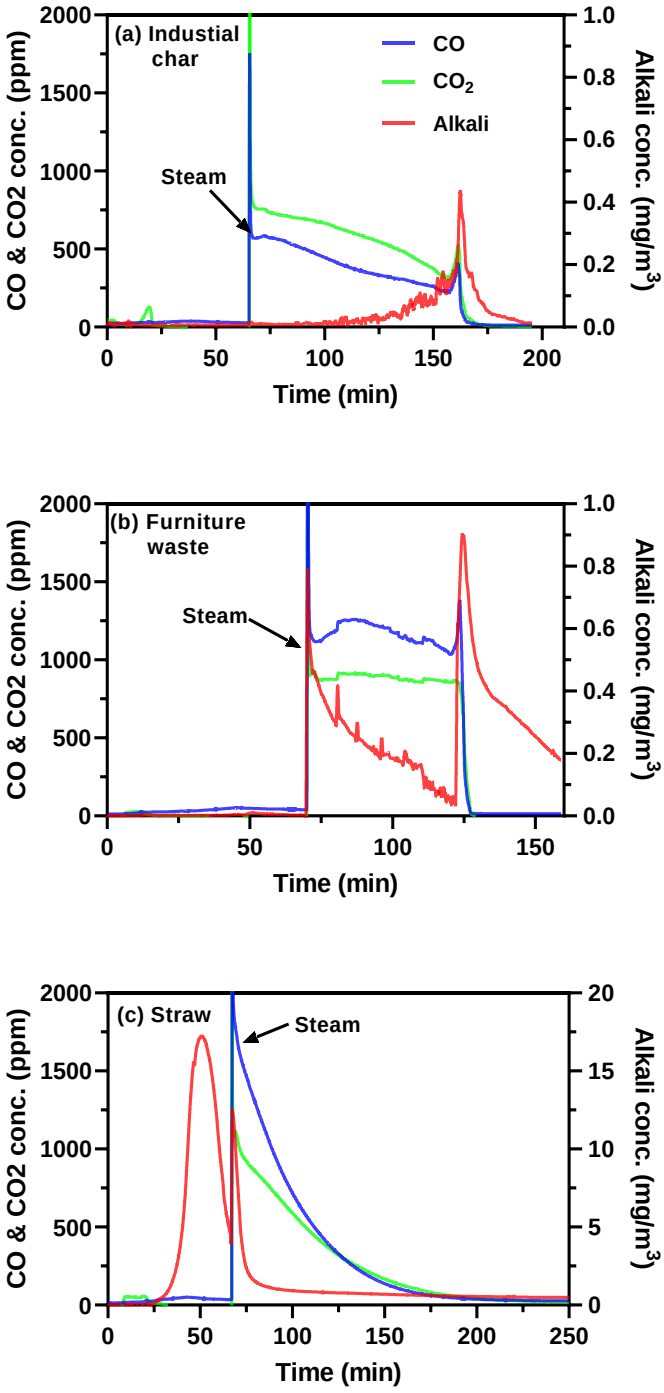

Figure 4.16 CO, CO_2 and alkali concentrations during isothermal gasification of: (a) industrial char; (b) furniture waste char; and (c) straw char, at 900°C. The black arrow indicates the time-points of steam injection. The char was heated in N_2 from room temperature to the designed gasification temperature before steam injection.

When steam is injected, all three chars show rapid increases in the CO and CO_2 concentrations, and this is followed by a decrease to lower concentrations. The CO and CO_2 concentrations of the OC slowly decrease until the final stage of gasification,

at which point they again increase for a short time and then suddenly decrease to zero. The CO and CO_2 concentrations of the furniture waste char remain relatively constant until the final stage of gasification, such that the behavior is the same as that observed for the OC. In contrast, the CO and CO_2 concentrations of the straw char continuously decrease throughout the gasification process. The significant difference in char conversion between wood char and straw char can be attributed to the latter having a high content of silicon, resulting in alkali deactivation [58]. In addition, for the OC, the CO_2 concentration is higher than the CO concentration, which is different from the other two biomass chars. The reason for this could be that the longer gasification time (low gasification reactivity) of the OC results in the gasification having a higher steam to carbon ratio throughout the process (total amount of introduced steam divided by the char mass). The level of alkali release from the furniture waste suddenly increases when steam is injected and continuously decreases until the final stage, at which point the alkali release increases once again. The trend of the alkali release is similar to the result seen for CO_2 gasification of the same material (Figure 4.1). However, the concentration of alkali at low conversions seems higher than that seen in the CO_2 gasification, since steam promotes the formation of easily released alkali hydroxides. The level of alkali release during straw char gasification is significantly different from that the levels observed during gasification of the two wood chars, and it rapidly decreases at the beginning and slowly decreases until the gasification is completed. The pattern of alkali release during straw char gasification is also different from that during CO_2 gasification, and the latter decays slowly throughout the process.

4.6 Pressurized gasification experiment

The experiments were carried out using the KTH pressurized gasifier shown in Figure 3.4, and the measuring system shown in Figure 3.5 was employed to measure the syngas composition, alkali concentration, and particle concentrations. Here, we show the results from a typical experiment conducted at a pressure of 5 bar and using oxygen as the gasifying agent.

The operational conditions, including biomass and gas feeding levels and temperature of the gasifier, are shown in Figure 4.17. Before fuel feeding was started at 18:42 (hh:mm), the gasifier was preheated to 890°C by the combustion of H_2, and more than 110 Nl/min N_2 were injected to maintain the pressure of the gasifier at 5 bar. After starting the fuel feed, the H_2 flow was gradually decreased and the O_2 flow was increased. The temperature of the gasifier experienced a drop, and this was followed by a new increase when the fuel feed was initiated. At around 18:50, the gasification reached a relatively stable state, which was maintained for approximately 30 min. Thereafter, the temperature increased rapidly, and the N_2 flows were increased to try to stabilize the temperature. However, the temperature climbed to above 1050°C and the thermocouples lost the signal at 19:35. The

experiment was shut down at 19:40, as indicated by the decreases in N_2 flow, O_2 flow and fuel feeding.

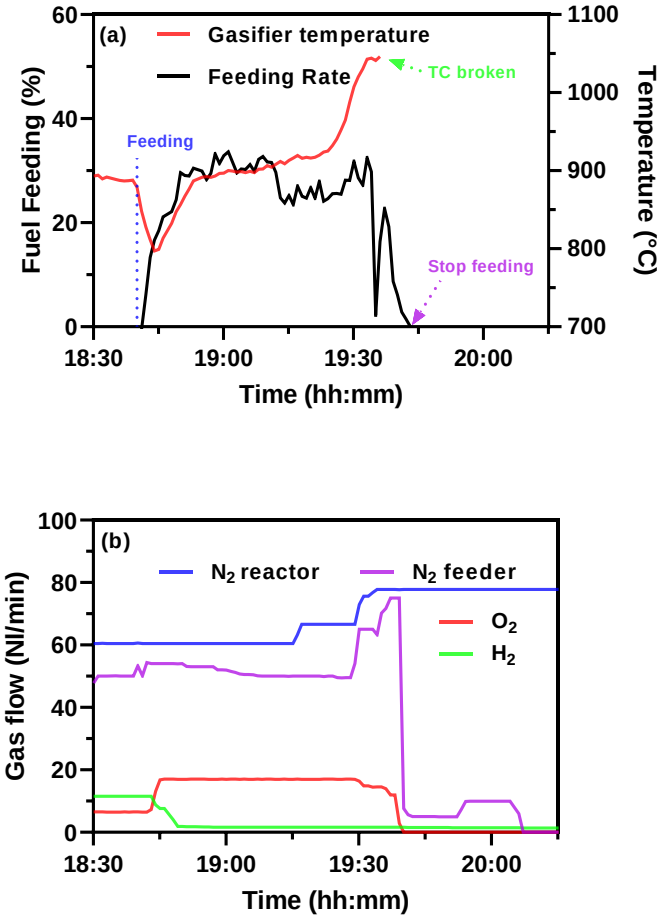

Figure 4.17 (a) Fuel feeding and temperature profile of the pressurized gasifier. (b) The flows of N_2, O_2, and H_2 injected into the gasifier during the experiment. N_2 was injected directly into the gasifier and via the feeder. Fuel feeding is the signal for a feeding indicator, and the value does not correspond to a feeding rate.

The results obtained from the experiment are shown in Figure 4.18. The flows of the syngas compounds CO, H_2, CO_2, and CH_4 increase when the feeding of biomass starts at 18:42. The alkali and particle concentrations also increased. At 19:15, the alkali and particle concentrations increase remarkably, which corresponds to the increases in gasifier temperature and N_2 flow for cooling (Figure 4.17). At the same time, the flow of CO increased, while the flow of the other main components in the syngas, i.e. H_2, CO_2, and CH_4, decreased. The variations in measured compositions after 19:15 are attributed to the high temperature, which influences exothermic reactions, e.g., the water-gas shift reaction, and endothermic reactions, e.g., methane reforming [158]. Following the rapid increases in alkali and particle concentrations, the levels continued to vary depending on changes in the gasifier temperature and N_2 flow. At 19:40, the gasifier was shut down due to overheating, and the alkali and

particle concentrations unexpectedly increased, before slowly decaying during the following 30 min. The observed increase may be related to the stop in N_2 flow in the feeder (Figure 4.17), as it has a reverse flow direction when injected compared to the reactor N_2 flow. Therefore, with only the N_2 reactor flow more particles and alkali may be transported out of the gasifier.

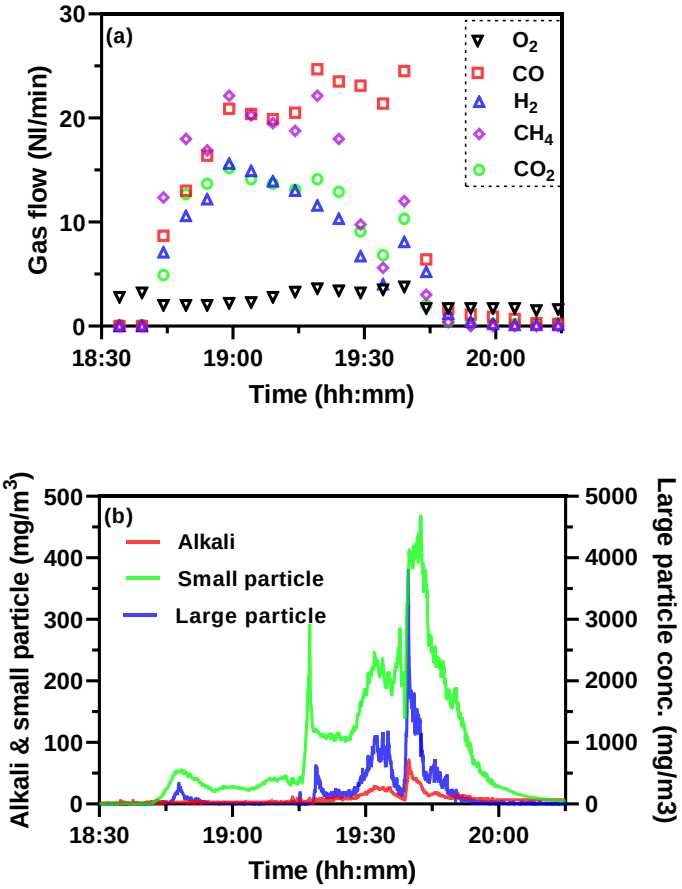

Figure 4.18 (a) Flow of CO, CO_2, H_2, CH_4, and O_2 and (b) concentrations of alkali, small (10.7 - 478 nm), and large (575–8750 nm) aerosol particles in the syngas produced by the gasifier.

The pilot experiment carried out online monitoring of alkali and particle concentrations in a pressurized gasifier, which to our knowledge is the first time that this has been achieved. This successful experiment confirms the validity of the measurement system depicted in Figure 3.5. The results show that the emissions profiles of alkali and particles are closely linked to the operation of the pressurized gasifier, including the influences of temperature and gas flow.

Chapter 5
Conclusions

This thesis presents the results for alkali measurements, particle measurements, and fuel conversion during biomass pyrolysis and char gasification. A reliable methodology for simultaneously detecting alkali release and sample mass during thermal conversion of fuels is created by connecting a surface ionization detector (SID), used for online alkali measurements, to a commercial thermogravimetric analyzer (TGA). In addition, a system based on diluters, a CO/CO_2 analyzer, a scan mobility particle sizer, an optical particle sizer, and an SID is successfully applied for particle and alkali measurements in laboratory- and pilot-scale reactors.

Real-time alkali release during the CO_2 gasification of different types of biochar, assessed using the TGA-SID, shows significantly different release profiles for wood char and straw char. Alkali release from wood char remains low and constant during most of the gasification process, whereas it increases remarkably during the final stage of gasification. This indicates that alkali is enriched during the process, prior to the final alkali release. In contrast, alkali release from straw char decreases continuously during the gasification process, which corresponds to conversion of the fuel. A high temperature and high CO_2 concentration promote char gasification and result in a higher level of alkali release. For chars with different alkali contents (and otherwise similar properties), the reactivity and alkali release levels during char gasification increase with the increase in alkali content of the char.

Co-conversion of wood and straw has clear effects on fuel conversion and alkali release. Using the TGA-SID setup and SEM-EDS, gas-phase alkali migration from the straw to the wood is observed at temperatures >600°C during co-pyrolysis. Due to the alkali migration, there is a positive synergistic effect during the subsequent co-gasification of their chars. A gasification temperature of 900°C and a wood content of 75% represent the conditions that produce the most-pronounced synergistic effect. Migration of silicon from the straw to the wood results in negative synergistic effects during the final stage of the gasification.

Different types of fresh bed materials have different effects on alkali release and fuel conversion during wood pyrolysis and char gasification. The investigated bed materials include silica, sea sand, olivine, ilmenite, alumina and dolomite. Dolomite reduces the total mass loss and alkali release at 200–400°C during pyrolysis, since the former can adsorb some volatiles. The adsorbed compounds decompose in the temperature range of 600–720°C, resulting in a small peak for mass loss. Sea sand and alumina enhance char reactivity during the whole or most of the gasification

stage, owing to their high alkali contents. Dolomite increases char reactivity at the beginning of gasification, due to some carbon deposits formed during pyrolysis. With the exception of alumina, the other bed materials inhibit alkali release and char reactivity when the char conversion approaches completion, which is attributed to silicon or titanium migration. Dolomite also increases alkali release during most of the gasification stage because the migrated Mg and Ca combine with silicates to ensure that more alkali survives in releasable forms. The effects of the six bed materials on straw char gasification are largely similar to those of wood char gasification, although some features are different due to the high alkali and silicon contents of the straw.

The bed material used for the thermal conversion of biomass over a period of days can result in the deposition of some AAEMs on the bed material surface, which in turn affects char conversion. Using the online alkali measurements, gas-phase alkali migration from used bed material to industrial char is observed. The SEM-EDS results show that other elements, i.e., Mg, Si, and Ca, which are abundant in the coating layer of the used bed material, can also move to the char surface. Char reactivity increases after mixing with used bed material during the initial stage of gasification owing to the catalytic effects of the migrated AAEMs. Alkali release increases because the migrated Mg and Ca allow more alkali to survive in releasable forms. However, the levels of char conversion rate and alkali release are significantly reduced during the final stage of gasification because the migrated silicon reacts chemically with the alkali to form stable compounds.

The levels of alkali and particle release during steam gasification of chars have also been measured using the comprehensive system. Industrial char and furniture waste char release significant amounts of alkali when char conversion approaches completion, in a manner similar to that observed in CO_2 gasification. However, before the final stage of char conversion, industrial char and furniture waste char show totally different alkali release behaviors. Alkali release from straw char decreases throughout the gasification process. The trend for particle concentration is similar to that for alkali release during steam gasification of the industrial char.

The measurement of alkali and particle release during biomass gasification in a pressurized gasifier has been successfully carried out. The results show that the emissions of alkali and particles are closely linked to the operation of pressurized gasifier. Additional experiments with different pressures and alternative gasifying agents need to be compared to acquire a comprehensive understanding of the pressurized gasification of biomass.

The studies of this thesis confirm that element migration, between biomasses or between biomass and bed material, occurs during the thermochemical conversion of biomass. The migration of AAEMs can facilitate the gasification of a biomass that accepts the elements, as is the case in the gasification of wood-straw blends, and the addition of used bed materials to industrial char. Some elements, including Si, Al

and Ti, can also migrate during the thermochemical conversion of biomass, as illustrated by the studies of fresh bed material, used bed material, and co-conversion. However, these elements may be combined with AAEMs to reduce the catalytic effect, resulting in reduced gasification reactivity. The migration of elements potentially occurs through both the gas phase and the transfer of melted material.

This thesis provides abundant new information about alkali release, element migration, and particle release during different biomass thermal conversion processes, i.e., CO_2 gasification, steam gasification, co-pyrolysis/gasification, mixing with fresh bed materials, and mixing with used bed materials. The results provide valuable information and knowledge that can be applied to industrial processes, in relation to alkali release during gasification, bed material selection, and co-conversion of fuels. Further studies that include the impacts of other parameters, e.g., structure and alkaline earth metals, on char gasification are prerequisites for building a kinetic model of char conversion and alkali release during gasification. Some aspects of the process, e.g., co-gasification and the effects of bed materials, need to be evaluated in a fluidized bed to reveal the effects of gas-solid interactions. Further development of the online alkali measurement method may also prove valuable, e.g., to allow differentiation between potassium and sodium. The effects of alkali earth metals on alkali release from straw also need to be studied further, e.g., by comparing the effects of MgO and CaO.

Acknowledgements

This interesting research project related to alkali release during biomass thermal conversion could not have been successfully completed without the help of many people.

First of all, I would like to thank my supervisor, Prof. Jan Pettersson, for giving me the opportunity to study in your group. Although you are often busy with your official work, you still spend as much time as you can working on our biomass conversion research. I enjoy the discussions with you about experiments, data analysis, and paper writing. I hope that we can continue to work together over the next few months to transform all our manuscripts to published papers. My thanks also to my co-supervisor, Dr. Xiangrui Kong, for devoting much time to campaigns, paper reviewing, and suggestions. I really appreciate the help that you gave me when I first arrived in Gothenburg and faced several challenges. I would like to thank my examiner, Prof. Mattias Hallquist, for all his support of my study plan and for course suggestions.

This work would not have been as successful without the help from my colleagues at KTH: Prof. Klas Engvall, Dr. Efthymios Kantarelis, Christer Rosén, and Saiman Ding. Klas, thank you for providing the instruments to perform the experiments, for covering most of my accommodation fees in Stockholm, and for your SFC project. Efthymios, thank you for your help with the catalyst test and for the suggestions regarding other tests. Christer, thank you for all your help with the test at the M building, instrument loading, and instrument packing-up. Saiman: we did most of our TGA and lab-scale reactor tests together, thanks for all your help when I was in Stockholm.

I am grateful to all the people in the Atmospheric Science group for their kind help. I thank Viktor for his help with the TGA test at Chalmers. Thanks to all the people who shared their research at the Monday meetings, allowing me to acquire valuable new knowledge of atmospheric science.

I also want to thank my parents for supporting me in my decision to quit IET, CAS and start a new journey to Sweden 4 years ago.

I would like to thank my dear friends and previous colleagues in China. Thanks for discussing and sharing hometown news with me, and for making me feel not so far away from home.

Finally and most importantly, to all readers, thanks for your interest in this thesis!

葛亚昕 (Ge,Yaxin)

July 2022, Gothenburg, Sweden

References

[1] Saxena RC, Adhikari DK, Goyal HB. Biomass-based energy fuel through biochemical routes: A review. Renew Sustain Energy Rev 2009;13:167–78. https://doi.org/10.1016/j.rser.2007.07.011.

[2] Lou R, Wu S bin. Products properties from fast pyrolysis of enzymatic/mild acidolysis lignin. Appl Energy 2011;88:316–22. https://doi.org/10.1016/j.apenergy.2010.06.028.

[3] Lauri P, Havlík P, Kindermann G, Forsell N, Böttcher H, Obersteiner M. Woody biomass energy potential in 2050. Energy Policy 2014;66:19–31. https://doi.org/10.1016/j.enpol.2013.11.033.

[4] Wu D, Wang Y, Wang Y, Li S, Wei X. Release of alkali metals during co-firing biomass and coal. Renew Energy 2016;96:91–7. https://doi.org/10.1016/j.renene.2016.04.047.

[5] Nielsen HP, Frandsen FJ, Dam-Johansen K, Baxter LL. Implications of chlorine-associated corrosion on the operation of biomass-fired boilers. Prog Energy Combust Sci 2000;26:283–98. https://doi.org/10.1016/S0360-1285(00)00003-4.

[6] Wellinger M, Biollaz S, Wochele J, Ludwig C. Sampling and online analysis of alkalis in thermal process gases with a novel surface ionization detector. Energy Fuels 2011;25:4163–71. https://doi.org/10.1021/ef200811q.

[7] Nurk G, Huthwelker T, Braun A, Ludwig C, Lust E, Struis RPWJ. Redox dynamics of sulphur with Ni/GDC anode during SOFC operation at mid- and low-range temperatures: An operando S K-edge XANES study. J Power Sources 2013;240:448–57. https://doi.org/10.1016/j.jpowsour.2013.03.187.

[8] Norheim A, Lindberg D, Hustad JE, Backman R. Equilibrium calculations of the composition of trace compounds from biomass gasification in the solid oxide fuel cell operating temperature interval. Energy Fuels 2009;23:920–5. https://doi.org/10.1021/ef800828m.

[9] Larsson A, Hedenskog M, Thunman H. Monitoring the bed material activation in the GoBiGas-gasifier. Nord Flame Days 2015 Copenhagen 2015.

[10] Wang C, Wu Y, Liu Q, Yang H, Wang F. Analysis of the behaviour of pollutant gas emissions during wheat straw/coal cofiring by TG-FTIR. Fuel Process Technol 2011;92:1037–41. https://doi.org/10.1016/j.fuproc.2010.12.029.

[11] Tillman DA. Biomass cofiring: The technology, the experience, the combustion consequences. Biomass Bioenergy 2000;19:365–84. https://doi.org/10.1016/S0961-9534(00)00049-0.

[12] Sami M, Annamalai K, Wooldridge M. Co-firing of coal and biomass fuel blends. Prog Energy Combust Sci 2001;27:171–214. https://doi.org/10.1016/S0360-1285(00)00020-4.

[13] Agbor E, Zhang X, Kumar A. A review of biomass co-firing in North America. Renew Sustain Energy Rev 2014;40:930–43. https://doi.org/10.1016/j.rser.2014.07.195.

[14] Sahu SG, Chakraborty N, Sarkar P. Coal-biomass co-combustion: An overview. Renew Sustain Energy Rev 2014;39:575–86. https://doi.org/10.1016/j.rser.2014.07.106.

[15] Wei J, Wang M, Wang F, Song X, Yu G, Liu Y, et al. A review on reactivity characteristics and synergy behavior of biomass and coal co-gasification. Int J Hydrogen Energy 2021;46:17116–32. https://doi.org/10.1016/j.ijhydene.2021.02.162.

[16] Wang M, Wan Y, Guo Q, Bai Y, Yu G, Liu Y, et al. Brief review on petroleum coke and biomass/coal co-gasification: Syngas production, reactivity characteristics, and synergy behavior. Fuel 2021;304:121517. https://doi.org/10.1016/j.fuel.2021.121517.

[17] Lv P, Bai Y, Wang J, Song X, Su W, Yu G, et al. Investigation into the interaction of biomass waste with industrial solid waste during co-pyrolysis and the synergetic effect of its char gasification. Biomass Bioenergy 2022;159:106414. https://doi.org/10.1016/j.biombioe.2022.106414.
[18] Zhou L, Zhang G, Reinmöller M, Meyer B. Effect of inherent mineral matter on the co-pyrolysis of highly reactive brown coal and wheat straw. Fuel 2019;239:1194–203. https://doi.org/10.1016/j.fuel.2018.11.114.
[19] Wei J, Song X, Guo Q, Ding L, Yoshikawa K, Yu G. Reactivity, synergy, and kinetics analysis of CO_2 co-pyrolysis/co-gasification of biomass after hydrothermal treatment and coal blends. Energy Fuels 2020;34:294–303. https://doi.org/10.1021/acs.energyfuels.9b03721.
[20] Lahijani P, Zainal ZA, Mohamed AR, Mohammadi M. Co-gasification of tire and biomass for enhancement of tire-char reactivity in CO_2 gasification process. Bioresour Technol 2013;138:124–30. https://doi.org/10.1016/j.biortech.2013.03.179.
[21] Wei J, Gong Y, Guo Q, Chen X, Ding L, Yu G. A mechanism investigation of synergy behaviour variations during blended char co-gasification of biomass and different rank coals. Renew Energy 2019;131:597–605. https://doi.org/10.1016/j.renene.2018.07.075.
[22] Zhang Y, Zheng Y, Yang M, Song Y. Effect of fuel origin on synergy during co-gasification of biomass and coal in CO_2. Bioresour Technol 2016;200:789–94. https://doi.org/10.1016/j.biortech.2015.10.076.
[23] Zhou C, Rosén C, Engvall K. Biomass oxygen/steam gasification in a pressurized bubbling fluidized bed: Agglomeration behavior. Appl Energy 2016;172:230–50. https://doi.org/10.1016/j.apenergy.2016.03.106.
[24] Corella J, Toledo JM, Padilla R. Olivine or dolomite as in-bed additive in biomass gasification with air in a fluidized bed: Which is better? Energy Fuels 2004;18:713–20. https://doi.org/10.1021/ef0340918.
[25] Devi L, Ptasinski KJ, Janssen FJJG, Van Paasen SVB, Bergman PCA, Kiel JHA. Catalytic decomposition of biomass tars: Use of dolomite and untreated olivine. Renew Energy 2005;30:565–87. https://doi.org/10.1016/j.renene.2004.07.014.
[26] Karatas H, Olgun H, Akgun F. Coal and coal and calcined dolomite gasification experiments in a bubbling fluidized bed gasifier under air atmosphere. Fuel Process Technol 2013;106:666–72. https://doi.org/10.1016/j.fuproc.2012.09.063.
[27] Marinkovic J, Thunman H, Knutsson P, Seemann M. Characteristics of olivine as a bed material in an indirect biomass gasifier. Chem Eng J 2015;279:555–66. https://doi.org/10.1016/j.cej.2015.05.061.
[28] Kirnbauer F, Wilk V, Kitzler H, Kern S, Hofbauer H. The positive effects of bed material coating on tar reduction in a dual fluidized bed gasifier. Fuel 2012;95:553–62. https://doi.org/10.1016/j.fuel.2011.10.066.
[29] Kuba M, Skoglund N, Öhman M, Hofbauer H. A review on bed material particle layer formation and its positive influence on the performance of thermo-chemical biomass conversion in fluidized beds. Fuel 2021;291. https://doi.org/10.1016/j.fuel.2021.120214.
[30] He H, Ji X, Boström D, Backman R, Öhman M. Mechanism of quartz bed particle layer formation in fluidized bed combustion of wood-derived fuels. Energy Fuels 2016;30:2227–32. https://doi.org/10.1021/acs.energyfuels.5b02891.
[31] He H, Boström D, Öhman M. Time dependence of bed particle layer formation in fluidized quartz bed combustion of wood-derived fuels. Energy Fuels 2014;28:3841–8.

https://doi.org/10.1021/ef500386k.
[32] Vilches TB, Marinkovic J, Seemann M, Thunman H. Comparing active bed materials in a dual fluidized bed biomass gasifier: Olivine, bauxite, quartz-Sand, and ilmenite. Energy Fuels 2016;30:4848–57. https://doi.org/10.1021/acs.energyfuels.6b00327.
[33] Corcoran A, Knutsson P, Lind F, Thunman H. Mechanism for migration and layer growth of biomass ash on ilmenite used for oxygen carrier aided combustion. Energy Fuels 2018;32:8845–56. https://doi.org/10.1021/acs.energyfuels.8b01888.
[34] Vilches TB, Maric J, Knutsson P, Rosenfeld DC, Thunman H, Seemann M. Bed material as a catalyst for char gasification: The case of ash-coated olivine activated by K and S addition. Fuel 2018;224:85–93. https://doi.org/10.1016/j.fuel.2018.03.079.
[35] Knutsson P, Maric J, Knutsson J, Larsson A, Breitholtz C, Seemann M. Potassium speciation and distribution for the K_2CO_3 additive-induced activation/deactivation of olivine during gasification of woody biomass. Appl Energy 2019;248:538–44. https://doi.org/10.1016/j.apenergy.2019.04.150.
[36] He H, Skoglund N, Öhman M. Time-dependent crack layer formation in quartz bed particles during fluidized bed combustion of woody biomass. Energy Fuels 2017;31:1672–7. https://doi.org/10.1021/acs.energyfuels.6b02980.
[37] Lundberg L, Tchoffor PA, Pallarès D, Thunman H, Davidsson KO. Impacts of bed material activation and fuel moisture content on the gasification rate of biomass char in a fluidized bed. Ind Eng Chem Res 2019;58:4802–9. https://doi.org/10.1021/acs.iecr.9b00528.
[38] Zhang Z, Liu J, Shen F, Wang Z. Temporal release behavior of potassium during pyrolysis and gasification of sawdust particles. Renew Energy 2020;156:98–106. https://doi.org/10.1016/j.renene.2020.04.076.
[39] Davidsson KO, Korsgren JG, Pettersson JBC, Jäglid U. The effects of fuel washing techniques on alkali release from biomass. Fuel 2002;81:137–42. https://doi.org/10.1016/S0016-2361(01)00132-6.
[40] Davidsson KO, Stojkova BJ, Pettersson JBC. Alkali emission from birchwood particles during rapid pyrolysis. Energy Fuels 2002;16:1033–9. https://doi.org/10.1021/ef010257y.
[41] Kulichkova GI, Ivanova TS, Köttner M, Volodko OI, Spivak SI, Tsygankov SP, et al. Plant feedstocks and their biogas production potentials. Open Agric J 2020;14:219–34. https://doi.org/10.2174/1874331502014010219.
[42] Luo Z, Zhou J. Handbook of climate change mitigation and adaptation. 2022. https://doi.org/10.1007/978-3-030-72579-2.
[43] Nunes LJR, Causer TP, Ciolkosz D. Biomass for energy: A review on supply chain management models. Renew Sustain Energy Rev 2020;120:109658. https://doi.org/10.1016/j.rser.2019.109658.
[44] Chhiti Y, Kemiha M. Thermal conversion of biomass, pyrolysis and gasification: a review. Int J Eng Sci 2013;2:75–85.
[45] Xiang Y, Cai L, Guan Y, Liu W, Cheng Z, Liu Z. Study on the effect of gasification agents on the integrated system of biomass gasification combined cycle and oxy-fuel combustion. Energy 2020;206:118131. https://doi.org/10.1016/j.energy.2020.118131.
[46] Hameed Z, Aslam M, Khan Z, Maqsood K, Atabani AE, Ghauri M, et al. Gasification of municipal solid waste blends with biomass for energy production and resources recovery: Current status, hybrid technologies and innovative prospects. Renew Sustain Energy Rev 2021;136:110375. https://doi.org/10.1016/j.rser.2020.110375.
[47] Andersson V, Ge Y, Kong X, Pettersson JBC. A novel method for on-line

characterization of alkali release and thermal stability of materials used in thermochemical conversion processes. Energies 2022;15. https://doi.org/10.3390/en15124365.

[48] Dastidar MG, Sarkar BK, Mitra MK, Dey R. Effect of alkali on different iron making processes. Mater Sci Eng Int J 2018;2:304–13. https://doi.org/10.15406/mseij.2018.02.00075.

[49] Mei Y, Wang Z, Zhang S, Fang Y. Novel assumption about the mechanism of catalytic gasification: on the basis of the same catalytic effect of alkali between C-CO_2 and Fe-CO_2 Reactions. Energy Fuels 2021;35:16258–63. https://doi.org/10.1021/acs.energyfuels.1c02159.

[50] Mitsuoka K, Hayashi S, Amano H, Kayahara K, Sasaoaka E, Uddin MA. Gasification of woody biomass char with CO_2: The catalytic effects of K and Ca species on char gasification reactivity. Fuel Process Technol 2011;92:26–31. https://doi.org/10.1016/j.fuproc.2010.08.015.

[51] Sadhwani N, Adhikari S, Eden MR, Wang Z, Baker R. Southern pines char gasification with CO_2—Kinetics and effect of alkali and alkaline earth metals. Fuel Process Technol 2016;150:64–70. https://doi.org/10.1016/j.fuproc.2016.04.037.

[52] Kirtania K, Axelsson J, Matsakas L, Christakopoulos P, Umeki K, Furusjö E. Kinetic study of catalytic gasification of wood char impregnated with different alkali salts. Energy 2017;118:1055–65. https://doi.org/10.1016/j.energy.2016.10.134.

[53] Feng D, Zhao Y, Zhang Y, Sun S, Gao J. Steam gasification of sawdust biochar influenced by chemical speciation of alkali and alkaline earth metallic species. Energies 2018;11. https://doi.org/10.3390/en11010205.

[54] Dahou T, Defoort F, Jeguirim M, Dupont C. Towards understanding the role of K during biomass steam gasification. Fuel 2020;282:118806. https://doi.org/10.1016/j.fuel.2020.118806.

[55] Klopper L, Strydom CA, Bunt JR. Influence of added potassium and sodium carbonates on CO_2 reactivity of the char from a demineralized inertinite rich bituminous coal. J Anal Appl Pyrolysis 2012;96:188–95. https://doi.org/10.1016/j.jaap.2012.04.005.

[56] Perander M, DeMartini N, Brink A, Kramb J, Karlström O, Hemming J, et al. Catalytic effect of Ca and K on CO_2 gasification of spruce wood char. Fuel 2015;150:464–72. https://doi.org/10.1016/j.fuel.2015.02.062.

[57] Zhao S, Ding L, Ruan Y, Bai B, Qiu Z, Li Z. Experimental and kinetic studies on steam gasification of a biomass char. Energies 2021;14. https://doi.org/10.3390/en14217229.

[58] Yu J, Guo Q, Gong Y, Ding L, Wang J, Yu G. A review of the effects of alkali and alkaline earth metal species on biomass gasification. Fuel Process Technol 2021;214:106723. https://doi.org/10.1016/j.fuproc.2021.106723.

[59] Dupont C, Nocquet T, Da Costa JA, Verne-Tournon C. Kinetic modelling of steam gasification of various woody biomass chars: Influence of inorganic elements. Bioresour Technol 2011;102:9743–8. https://doi.org/10.1016/j.biortech.2011.07.016.

[60] Dupont C, Jacob S, Marrakchy KO, Hognon C, Grateau M, Labalette F, et al. How inorganic elements of biomass influence char steam gasification kinetics. Energy 2016;109:430–5. https://doi.org/10.1016/j.energy.2016.04.094.

[61] Suzuki T, Nakajima H, Ikenaga N oki, Oda H, Miyake T. Effect of mineral matters in biomass on the gasification rate of their chars. Biomass Convers Biorefin 2011;1:17–28. https://doi.org/10.1007/s13399-011-0006-2.

[62] Karlström O, Dirbeba MJ, Costa M, Brink A, Hupa M. Influence of K/C ratio on gasification rate of biomass chars. Energy Fuels 2018;32:10695–700. https://doi.org/10.1021/acs.energyfuels.8b02288.
[63] Davidsson KO, Åmand LE, Steenari BM, Elled AL, Eskilsson D, Leckner B. Countermeasures against alkali-related problems during combustion of biomass in a circulating fluidized bed boiler. Chem Eng Sci 2008;63:5314–29. https://doi.org/10.1016/j.ces.2008.07.012.
[64] Hirohata O, Wakabayashi T, Tasaka K, Fushimi C, Furusawa T. Release behavior of tar and alkali and alkaline earth metals during biomass steam gasification. Energy Fuels 2008:4235–9. https://doi.org/10.1021/ef800390n
[65] Keown DM, Hayashi JI, Li CZ. Drastic changes in biomass char structure and reactivity upon contact with steam. Fuel 2008;87:1127–32. https://doi.org/10.1016/j.fuel.2007.05.057.
[66] Jiang L, Hu S, Xiang J, Su S, Su L-S, Xu K, et al. Release characteristics of alkali and alkaline earth metallic species during biomass pyrolysis and steam gasification process. Bioresour Technol 2012;116:278–84. https://doi.org/10.1016/j.biortech.2012.03.051.
[67] Yang T, Jia K, Kai X, Sun Y, Li Y, Li R. A study on the migration behavior of K, Na, and Cl during biomass gasification. BioResources 2016;11:7133–44. https://doi.org/10.15376/biores.11.3.7133-7144.
[68] Fatehi H, He Y, Wang Z, Li ZS, Bai XS, Aldén M, et al. LIBS measurements and numerical studies of potassium release during biomass gasification. Proc Combust Inst 2015;35:2389–96. https://doi.org/10.1016/j.proci.2014.06.115.
[69] Zhang Z, Liu J, Shen F, Yang Y, Liu F. On-line measurement and kinetic studies of sodium release during biomass gasification and pyrolysis. Fuel 2016;178:202–8. https://doi.org/10.1016/j.fuel.2016.03.067.
[70] Zhang Z, Liu J, Shen F, Wang Z. Temporal release behavior of potassium during pyrolysis and gasification of sawdust particles. Renew Energy 2020;156:98–106. https://doi.org/10.1016/j.renene.2020.04.076.
[71] Park DK, Kim SD, Lee SH, Lee JG. Co-pyrolysis characteristics of sawdust and coal blend in TGA and a fixed bed reactor. Bioresour Technol 2010;101:6151–6. https://doi.org/10.1016/j.biortech.2010.02.087.
[72] Hu J, Si Y, Yang H, Shao J, Wang X, Lei T, et al. Influence of volatiles-char interactions between coal and biomass on the volatiles released, resulting char structure and reactivity during co-pyrolysis. Energy Convers Manag 2017;152:229–38. https://doi.org/10.1016/j.enconman.2017.09.051.
[73] Wei J, Gong Y, Guo Q, Ding L, Wang F, Yu G. Physicochemical evolution during rice straw and coal co-pyrolysis and its effect on co-gasification reactivity. Bioresour Technol 2017;227:345–52. https://doi.org/10.1016/j.biortech.2016.12.068.
[74] Krerkkaiwan S, Fushimi C, Tsutsumi A, Kuchonthara P. Synergetic effect during co-pyrolysis/gasification of biomass and sub-bituminous coal. Fuel Process Technol 2013;115:11–8. https://doi.org/10.1016/j.fuproc.2013.03.044.
[75] Ellis N, Masnadi MS, Roberts DG, Kochanek MA, Ilyushechkin AY. Mineral matter interactions during co-pyrolysis of coal and biomass and their impact on intrinsic char co-gasification reactivity. Chem Eng J 2015;279:402–8. https://doi.org/10.1016/j.cej.2015.05.057.
[76] Lu KM, Lee WJ, Chen WH, Lin TC. Thermogravimetric analysis and kinetics of co-

pyrolysis of raw/torrefied wood and coal blends. Appl Energy 2013;105:57–65. https://doi.org/10.1016/j.apenergy.2012.12.050.

[77] Yu J, Guo Q, Gong Y, Ding L, Wang J, Yu G. A review of the effects of alkali and alkaline earth metal species on biomass gasification. Fuel Process Technol 2021;214:106723. https://doi.org/10.1016/j.fuproc.2021.106723.

[78] Lu P, Huang Q, (Thanos) Bourtsalas AC, Chi Y, Yan J. Synergistic effects on char and oil produced by the co-pyrolysis of pine wood, polyethylene and polyvinyl chloride. Fuel 2018;230:359–67. https://doi.org/10.1016/j.fuel.2018.05.072.

[79] Fernandes R, Hill JM, Kopyscinski J. Determination of the synergism/antagonism parameters during co-gasification of potassium-rich biomass with non-biomass feedstock. Energy Fuels 2017;31:1842–9. https://doi.org/10.1021/acs.energyfuels.6b02270.

[80] Habibi R, Kopyscinski J, Masnadi MS, Lam J, Grace JR, Mims CA, et al. Co-gasification of biomass and non-biomass feedstocks: Synergistic and inhibition effects of switchgrass mixed with sub-bituminous coal and fluid coke during CO_2 gasification. Energy Fuels 2013;27:494–500. https://doi.org/10.1021/ef301567h.

[81] Satyam Naidu V, Aghalayam P, Jayanti S. Synergetic and inhibition effects in carbon dioxide gasification of blends of coals and biomass fuels of Indian origin. Bioresour Technol 2016;209:157–65. https://doi.org/10.1016/j.biortech.2016.02.137.

[82] Ding L, Zhang Y, Wang Z, Huang J, Fang Y. Interaction and its induced inhibiting or synergistic effects during co-gasification of coal char and biomass char. Bioresour Technol 2014;173:11–20. https://doi.org/10.1016/j.biortech.2014.09.007.

[83] Rizkiana J, Guan G, Widayatno WB, Hao X, Huang W, Tsutsumi A, et al. Effect of biomass type on the performance of cogasification of low rank coal with biomass at relatively low temperatures. Fuel 2014;134:414–9. https://doi.org/10.1016/j.fuel.2014.06.008.

[84] Kajitani S, Zhang Y, Umemoto S, Ashizawa M, Hara S. Co-gasification reactivity of coal and woody biomass in high-temperature gasification. Energy Fuels 2010;24:145–51. https://doi.org/10.1021/ef900526h.

[85] Lv J, Ao X, Li Q, Cao Y, Chen Q, Xie Y. Steam co-gasification of different ratios of spirit-based distillers' grains and anthracite coal to produce hydrogen-rich gas. Bioresour Technol 2019;283:59–66. https://doi.org/10.1016/j.biortech.2019.03.047.

[86] Ren H, Zhang Y, Fang Y, Wang Y. Co-gasification behavior of meat and bone meal char and coal char. Fuel Process Technol 2011;92:298–307. https://doi.org/10.1016/j.fuproc.2010.09.013.

[87] Jeong HJ, Hwang IS, Hwang J. Co-gasification of bituminous coal-pine sawdust blended char with H_2O at temperatures of 750-850°C. Fuel 2015;156:26–9. https://doi.org/10.1016/j.fuel.2015.04.018.

[88] Salour D, Jenkins BM, Vafaei M, Kayhanian M. Control of in-bed agglomeration by fuel blending in a pilot scale straw and wood fueled AFBC. Biomass Bioenergy 1993;4:117–33. https://doi.org/10.1016/0961-9534(93)90033-Z.

[89] Thy P, Jenkins BM, Williams RB, Lesher CE, Bakker RR. Bed agglomeration in fluidized combustor fueled by wood and rice straw blends. Fuel Process Technol 2010;91:1464–85. https://doi.org/10.1016/j.fuproc.2010.05.024.

[90] Link S, Yrjas P, Lindberg D, Trikkel A. Characterization of ash melting of reed and wheat straw blend. ACS Omega 2022;7:2137–46. https://doi.org/10.1021/acsomega.1c05087.

[91] Link S, Yrjas P, Lindberg D, Trikkel A, Mikli V. Ash melting behaviour of reed and woody fuels blends. Fuel 2022;314:123051. https://doi.org/10.1016/j.fuel.2021.123051.
[92] Link S, Yrjas P, Hupa L. Ash melting behaviour of wheat straw blends with wood and reed. Renew Energy 2018;124:11–20. https://doi.org/10.1016/j.renene.2017.09.050.
[93] Barmina I, Valdmanis R, Zake M. The effects of biomass co-gasification and co-firing on the development of combustion dynamics. Energy 2018;146:4–12. https://doi.org/10.1016/j.energy.2017.04.140.
[94] Zhao J, Wang S, Wu Z, Meng H, Chen L. Hydrogen-rich syngas produced from the co-pyrolysis of municipal solid waste and wheat straw. Int J Hydrogen Energy 2017;42:19701–8. https://doi.org/10.1016/j.ijhydene.2017.06.166.
[95] Valin S, Ravel S, Vincent P, Thiery S, Miller H, Defoort F, et al. Fluidised bed gasification of diverse biomass and feedstocks—An overall performance study. Energies 2020;13:3706. https://doi.org/10.3390/en13143706
[96] Nzihou A, Stanmore B, Sharrock P. A review of catalysts for the gasification of biomass char, with some reference to coal. Energy 2013;58:305–17. https://doi.org/10.1016/j.energy.2013.05.057.
[97] Li B, Magoua Mbeugang CF, Huang Y, Liu D, Wang Q, Zhang S. A review of CaO based catalysts for tar removal during biomass gasification. Energy 2022;244:123172. https://doi.org/10.1016/j.energy.2022.123172.
[98] Larsson A, Israelsson M, Lind F, Seemann M, Thunman H. Using ilmenite to reduce the tar yield in a dual fluidized bed gasification system. Energy Fuels 2014;28:2632–44. https://doi.org/10.1021/ef500132p.
[99] Vassilev S V., Vassileva CG, Song YC, Li WY, Feng J. Ash contents and ash-forming elements of biomass and their significance for solid biofuel combustion. Fuel 2017;208:377–409. https://doi.org/10.1016/j.fuel.2017.07.036.
[100] He H, Skoglund N, Öhman M. Time-dependent layer formation on K-feldspar bed particles during fluidized bed combustion of woody fuels. Energy Fuels 2017;31:12848–56. https://doi.org/10.1021/acs.energyfuels.7b02386.
[101] Faust R, Hannl TK, Vilches TB, Kuba M, Öhman M, Seemann M, et al. Layer formation on feldspar bed particles during indirect gasification of wood. 1. K-feldspar. Energy Fuels 2019;33:7321–32. https://doi.org/10.1021/acs.energyfuels.9b01291.
[102] Marinkovic J, Seemann M, Schwebel GL, Thunman H. Impact of biomass ash-bauxite bed interactions on an indirect biomass gasifier. Energy Fuels 2016;30:4044–52. https://doi.org/10.1021/acs.energyfuels.6b00157.
[103] Kern S, Pfeifer C, Hofbauer H. Reactivity tests of the water-gas shift reaction on fresh and used fluidized bed materials from industrial DFB biomass gasifiers. Biomass Bioenergy 2013;55:227–33. https://doi.org/10.1016/j.biombioe.2013.02.001.
[104] Kuba M, Havlik F, Kirnbauer F, Hofbauer H. Influence of bed material coatings on the water-gas-shift reaction and steam reforming of toluene as tar model compound of biomass gasification. Biomass Bioenergy 2016;89:40–9. https://doi.org/10.1016/j.biombioe.2015.11.029.
[105] Zhang Y, Wang J, Lv P, Bie N, Cao P, Bai Y, et al. Capture of released alkali metals and its simultaneously catalytic performance on secondary reactions of volatiles during biomass pyrolysis. Fuel 2022;317:123557. https://doi.org/10.1016/j.fuel.2022.123557.
[106] Puig-Gamero M, Lara-Díaz J, Valverde JL, Sanchez-Silva L, Sánchez P. Dolomite effect on steam co-gasification of olive pomace, coal and petcoke: TGA-MS analysis, reactivity and synergistic effect. Fuel 2018;234:142–50.

https://doi.org/10.1016/j.fuel.2018.07.014.
[107] Keller M, Leion H, Mattisson T. Mechanisms of solid fuel conversion by chemical-looping combustion (CLC) using manganese ore: Catalytic gasification by potassium compounds. Energy Technol 2013;1:273–82. https://doi.org/10.1002/ente.201200052.
[108] Aho A, DeMartini N, Pranovich A, Krogell J, Kumar N, Eränen K, et al. Pyrolysis of pine and gasification of pine chars - Influence of organically bound metals. Bioresour Technol 2013;128:22–9. https://doi.org/10.1016/j.biortech.2012.10.093.
[109] van Eyk PJ, Ashman PJ, Alwahabi ZT, Nathan GJ. The release of water-bound and organic sodium from Loy Yang coal during the combustion of single particles in a flat flame. Combust Flame 2011;158:1181–92. https://doi.org/10.1016/j.combustflame.2010.10.024.
[110] Kowalski T, Judex J, Schildhauer TJ, Ludwig C. Transmission of alkali aerosols through sampling systems. Chem Eng Technol 2011;34:42–8. https://doi.org/10.1002/ceat.201000366.
[111] Gall D, Nejman C, Allguren T, Andersson K, Pettersson JBC. A new technique for real-time measurements of potassium and sodium aerosols based on field-reversal surface ionization. Meas Sci Technol 2021;32. https://doi.org/10.1088/1361-6501/abe130.
[112] Olsson JG, Jäglid U, Pettersson JBC, Hald P. Alkali metal emission during pyrolysis of biomass. Energy Fuels 1997;11:779–84. https://doi.org/10.1021/ef960096b.
[113] Gogolev I, Linderholm C, Gall D, Schmitz M, Mattisson T, Pettersson JBC, et al. Chemical-looping combustion in a 100 kW unit using a mixture of synthetic and natural oxygen carriers – Operational results and fate of biomass fuel alkali. Int J Greenh Gas Control 2019;88:371–82. https://doi.org/10.1016/j.ijggc.2019.06.020.
[114] Andersson V, Soleimanisalim AH, Kong X, Leion H, Mattisson T, Pettersson JBC. Alkali interactions with a calcium manganite oxygen carrier used in chemical looping combustion. Fuel Process Technol 2022;227:107099. https://doi.org/10.1016/j.fuproc.2021.107099.
[115] Andersson V, Soleimanisalim AH, Kong X, Hildor F, Leion H, Mattisson T, et al. Alkali-wall interactions in a laboratory-scale reactor for chemical looping combustion studies. Fuel Process Technol 2021;217:106828. https://doi.org/10.1016/j.fuproc.2021.106828.
[116] Gogolev I, Pikkarainen T, Kauppinen J, Linderholm C, Steenari BM, Lyngfelt A. Investigation of biomass alkali release in a dual circulating fluidized bed chemical looping combustion system. Fuel 2021;297:120743. https://doi.org/10.1016/j.fuel.2021.120743.
[117] Gogolev I, Soleimanisalim AH, Linderholm C, Lyngfelt A. Commissioning, performance benchmarking, and investigation of alkali emissions in a 10 kWth solid fuel chemical looping combustion pilot. Fuel 2021;287:119530. https://doi.org/10.1016/j.fuel.2020.119530.
[118] Pushp M, Gall D, Davidsson K, Seemann M, Pettersson JBC. Influence of bed material, additives, and operational conditions on alkali metal and tar concentrations in fluidized bed gasification of biomass. Energy Fuels 2018;32:6797–806. https://doi.org/10.1021/acs.energyfuels.8b00159.
[119] Gall D, Pushp M, Larsson A, Davidsson K, Pettersson JBC. Online measurements of alkali metals during start-up and operation of an industrial-scale biomass gasification plant. Energy Fuels 2018;32:532–41. https://doi.org/10.1021/acs.energyfuels.7b03135.
[120] Ding S, Kantarelis E, Engvall K. Effects of porous structure development and ash on

the steam gasification reactivity of biochar residues from a commercial gasifier at different temperatures. Energies 2020;13. https://doi.org/10.3390/en13195004.
[121] Davidsson KO, Engvall K, Hagström M, Korsgren JG, Lönn B, Pettersson JBC. A surface ionization instrument for on-line measurements of alkali metal components in combustion: Instrument description and applications. Energy Fuels 2002;16:1369–77. https://doi.org/10.1021/ef020020h.
[122] Gall D, Viljanen J, Gogolev I, Allgurén T, Andersson K. Alkali monitoring of industrial process gas by surface ionization─Calibration, assessment, and comparison to in situ laser diagnostics. Energy Fuels 2021;35:20160–71. https://doi.org/10.1021/acs.energyfuels.1c03205.
[123] Kowalski T, Ludwig C, Wokaun A. Qualitative evaluation of alkali release during the pyrolysis of biomass. Energy Fuels 2007;21:3017–22. https://doi.org/10.1021/ef070094z.
[124] Gogolev I, Soleimanisalim AH, Mei D, Lyngfelt A. Effects of temperature, operation mode, and steam concentration on alkali release in chemical looping conversion of biomass experimental investigation in a 10 kWthPilot. Energy Fuels 2021. https://doi.org/10.1021/acs.energyfuels.1c04353.
[125] Dinoi A, Donateo A, Conte M, Conte M, Belosi F. Comparison of atmospheric particle concentration measurements using different optical detectors: Potentiality and limits for air quality applications. Meas J Int Meas Confed 2017;106:274–82. https://doi.org/10.1016/j.measurement.2016.02.019.
[126] Umeki K, Moilanen A, Gómez-Barea A, Konttinen J. A model of biomass char gasification describing the change in catalytic activity of ash. Chem Eng J 2012;207–208:616–24. https://doi.org/10.1016/j.cej.2012.07.025.
[127] Ding L, Gong Y, Wang Y, Wang F, Yu G. Characterisation of the morphological changes and interactions in char, slag and ash during CO_2 gasification of rice straw and lignite. Appl Energy 2017;195:713–24. https://doi.org/10.1016/j.apenergy.2017.03.098.
[128] Bouraoui Z, Dupont C, Jeguirim M, Limousy L, Gadiou R. CO_2 gasification of woody biomass chars: The influence of K and Si on char reactivity. Comptes Rendus Chimie 2016;19:457–65. https://doi.org/10.1016/j.crci.2015.08.012.
[129] Zhang Y, Ashizawa M, Kajitani S, Miura K. Proposal of a semi-empirical kinetic model to reconcile with gasification reactivity profiles of biomass chars. Fuel 2008;87:475–81. https://doi.org/10.1016/j.fuel.2007.04.026.
[130] Halim N, Tajima A, Asano S, Kudo S, Hayashi JI. Change in catalytic activity of potassium during CO_2 gasification of char. Energy Fuels 2020;34:225–34. https://doi.org/10.1021/acs.energyfuels.9b03630.
[131] Blasi C. Combustion and gasification rates of lignocellulosic chars. Prog Energy Combust Sci 2009;35:121–40. https://doi.org/10.1016/j.pecs.2008.08.001.
[132] Porbatzki D, Stemmler M, Müller M. Release of inorganic trace elements during gasification of wood, straw, and miscanthus. Biomass Bioenergy 2011;35:3–10. https://doi.org/10.1016/j.biombioe.2011.04.001.
[133] Zhang W, Huang S, Wu S, Wu Y, Gao J. Ash fusion characteristics and gasification activity during biomasses co-gasification process. Renew Energy 2020;147:1584–94. https://doi.org/10.1016/j.renene.2019.09.058.
[134] Reinmöller M, Schreiner M, Guhl S, Neuroth M, Meyer B. Ash behavior of various fuels: The role of the intrinsic distribution of ash species. Fuel 2019;253:930–40. https://doi.org/10.1016/j.fuel.2019.05.036.

[135] Bernardo P, Drioli E, Golemme G. Membrane gas separation: A review/state of the art. Ind Eng Chem Res 2009;48:4638–63. https://doi.org/10.1021/ie8019032.
[136] Zevenhoven-Onderwater M, Backman R, Skrifvars BJ, Hupa M, Liliendahl T, Rosén C, et al. The ash chemistry in fluidised bed gasification of biomass fuels. Part I: Predicting the chemistry of melting ashes and ash-bed material interaction. Fuel 2001;80:1489–502. https://doi.org/10.1016/S0016-2361(01)00026-6.
[137] Hedayati A, Sefidari H, Boman C, Skoglund N, Kienzl N, Öhman M. Ash transformation during single-pellet gasification of agricultural biomass with focus on potassium and phosphorus. Fuel Process Technol 2021;217. https://doi.org/10.1016/j.fuproc.2021.106805.
[138] Yu HY, Pan XL, Wang B, Zhang W, Sun HL, Bi SW. Effect of Na_2O on formation of calcium aluminates in CaO-Al_2O_3-SiO_2 system. Trans Nonferrous Met Soc China (English Ed 2012;22:3108–12. https://doi.org/10.1016/S1003-6326(11)61578-1.
[139] Kim DG, Konar B, Jung IH. Thermodynamic optimization of the K_2O-Al_2O_3-SiO_2 system. Ceram Int 2018;44:16712–24. https://doi.org/10.1016/j.ceramint.2018.06.099.
[140] Rebbling A, Fagerström J, Steinvall E, Carlborg M, Öhman M, Boman C. Reduction of alkali release by two fuel additives at different bed temperatures during grate combustion of woody biomass. Energy Fuels 2019;33:11041–8. https://doi.org/10.1021/acs.energyfuels.9b02391.
[141] Tanaka S, U-emura T, Ishizaki K ichi, Nagayoshi K, Ikenaga N oki, Ohme H, et al. CO_2 gasification of iron-loaded carbons: activation of the iron catalyst with CO. Energy Fuels 1995;9:45–52. https://doi.org/10.1021/ef00049a007.
[142] Li F, Yu B, Li J, Wang Z, Guo M, Fan H, et al. Exploration of potassium migration behavior in straw ashes under reducing atmosphere and its modification by additives. Renew Energy 2020;145:2286–95. https://doi.org/10.1016/j.renene.2019.07.141.
[143] Arnold RA, Habibi R, Kopyscinski J, Hill JM. Interaction of potassium and calcium in the catalytic gasification of biosolids and switchgrass. Energy Fuels 2017;31:6240–7. https://doi.org/10.1021/acs.energyfuels.7b00972.
[144] Jiang MQ, Zhou R, Hu J, Wang FC, Wang J. Calcium-promoted catalytic activity of potassium carbonate for steam gasification of coal char: Influences of calcium species. Fuel 2012;99:64–71. https://doi.org/10.1016/j.fuel.2012.04.007.
[145] Kuchonthara P, Vitidsant T, Tsutsumi A. Catalytic effects of potassium on lignin steam gasification with γ-Al_2O_3 as a bed material. Korean J Chem Eng 2008;25:656–62. https://doi.org/10.1007/s11814-008-0108-0.
[146] Hu J, Liu L, Cui M, Wang J. Calcium-promoted catalytic activity of potassium carbonate for gasification of coal char: The synergistic effect unrelated to mineral matter in coal. Fuel 2013;111:628–35. https://doi.org/10.1016/j.fuel.2013.03.038.
[147] Strandberg A, Carlborg M, Boman C, Broström M. Ash transformation during single-pellet combustion of a silicon-poor woody biomass. Energy Fuels 2019;33:7770–7. https://doi.org/10.1021/acs.energyfuels.9b00937.
[148] Ge Z, Cao X, Zha Z, Ma Y, Zeng M, Wu K, et al. The mineral transformation and molten behaviors of biomass waste ashes in gasification-melting process. Fuel Process Technol 2022;226:107095. https://doi.org/10.1016/j.fuproc.2021.107095.
[149] Zhang J, Tang J, Liu L, Wang J. The evolution of catalytically active calcium catalyst during steam gasification of lignite char. Carbon N Y 2021;172:162–73. https://doi.org/10.1016/j.carbon.2020.09.089.
[150] Liu L, Liu H, Cui M, Hu Y, Wang J. Calcium-promoted catalytic activity of potassium

carbonate for steam gasification of coal char: Transformations of sulfur. Fuel 2013;112:687–94. https://doi.org/10.1016/j.fuel.2012.06.048.

[151] Tang J, Guo R, Wang J. Inhibition of interaction between kaolinite and K_2CO_3 by pretreatment using calcium additive. J Therm Anal Calorim 2013;114:153–60. https://doi.org/10.1007/s10973-012-2905-2.

[152] Ramsurn H, Kumar S, Gupta RB. Enhancement of biochar gasification in alkali hydrothermal medium by passivation of inorganic components using $Ca(OH)_2$. Energy Fuels 2011;25:2389–98. https://doi.org/10.1021/ef200438b.

[153] D'Orazio A, Rapagnà S, Foscolo PU, Gallucci K, Nacken M, Heidenreich S, et al. Gas conditioning in H_2 rich syngas production by biomass steam gasification: Experimental comparison between three innovative ceramic filter candles. Int J Hydrogen Energy 2015;40:7282–90. https://doi.org/10.1016/j.ijhydene.2015.03.169.

[154] Suzuki T, Ohme H, Watanabe Y. Alkali metal catalyzed CO_2 gasification of carbon. Energy Fuels 1992;6:343–51. https://doi.org/10.1021/ef00034a003.

[155] Defoort F, Dupont C, Durruty J, Guillaudeau J, Bedel L, Ravel S, et al. Thermodynamic study of the alkali release behavior during steam gasification of several biomasses. Energy Fuels 2015;29:7242–53. https://doi.org/10.1021/acs.energyfuels.5b01755.

[156] Jiang L, Hu S, Xu K, Wang Y, Syed-Hassan SSA, Su S, et al. Formation, fates and roles of catalytic precursors generated from the K_2CO_3-carbon interactions in the K_2CO_3-catalyzed CO_2 gasification of coal char. J Anal Appl Pyrolysis 2017;124:384–92. https://doi.org/10.1016/j.jaap.2016.11.006.

[157] Ge Y, Ding S, Kong X, Kantarelis E, Engvall K, Pettersson JBC. Real-time monitoring of alkali release during CO_2 gasification of different types of biochar. Fuel 2022;327:125102. https://doi.org/10.1016/j.fuel.2022.125102.

[158] Cabello A, Mendiara T, Abad A, Izquierdo MT, García-Labiano F. Production of hydrogen by chemical looping reforming of methane and biogas using a reactive and durable Cu-based oxygen carrier. Fuel 2022;322:124250. https://doi.org/10.1016/j.fuel.2022.124250.

Part II
Papers